Climate Dynamics (2021) 57:1507–1531
https://doi.org/10.1007/s00382-021-05728-6

Future projections in tropical cyclone activity over multiple CORDEX domains from RegCM4 CORDEX-CORE simulations

José Abraham Torres-Alavez[1] · Russell Glazer[1] · Filippo Giorgi[1] · Erika Coppola[1] · Xuejie Gao[2] · Kevin I. Hodges[3] · Sushant Das[1] · Moetasim Ashfaq[4] · Marco Reale[1,5] · Taleena Sines[1]

Received: 22 July 2020 / Accepted: 9 March 2021 / Published online: 6 April 2021

Abstract

The characteristics of tropical cyclone (TC) activity over five TC basins lying within four Coordinated Regional Downscaling Experiment (CORDEX) domains are examined for present and future climate conditions using a new ensemble of simulations completed as part of the CORDEX-CORE initiative with the regional climate model RegCM4. The simulations are conducted at a 25 km horizontal grid spacing and are driven by three CMIP5 general circulation models (GCMs) under two Representative Concentration Pathways (RCP2.6 and RCP8.5). The RegCM4 captures most features of the observed TC climatology, except for the TC intensity, which is thus statistically adjusted using a bias correction procedure to account for the effect of the coarse model resolution. The RegCM4 exhibits an improved simulation of several TC statistics compared to the driving GCMs, over most basins analyzed. In future climate conditions we find significant increases in TC frequency over the North Indian Ocean, the Northwest Pacific and Eastern Pacific regions, which are consistent with an increase in mid-tropospheric relative humidity. The North Atlantic and Australasia regions show a decrease in TC frequency, mostly associated with an increase in wind shear. We also find a consistent increase in future storm rainfall rates associated with TCs and in the frequency of the most intense TCs over most domains. Our study shows robust responses often, but not always, in line with previous studies, still implying the presence of significant uncertainties in the projection of TC characteristics, which need to be addressed using large ensembles of simulations with high-resolution models.

Keywords Regional climate model · CORDEX-CORE · Tropical cyclones · Climate change

1 Introduction

Tropical cyclones (TCs) have a wide-ranging socioeconomic impact (Camargo and Wing 2016; Knutson et al. 2019), mostly related to the destructive effects of their intense winds, storm surges, and extreme precipitation. They also play a beneficial role in providing freshwater for agriculture and other water resources (Czajkowski et al. 2013; Rappaport 2000; Dominguez and Magaña 2018). Therefore, increasing our knowledge of how TC characteristics could change with anthropogenic warming is critical to assessing their impacts on human and natural systems and to developing suitable adaptation and mitigation strategies.

Recently, numerous studies have examined how TC genesis, occurrence, maximum wind speed and mean precipitation could change under warmer conditions. These have used General Circulation Models (GCMs; Bengtsson et al. 2007; Camargo 2013; Murakami et al. 2012a, b, 2014; Knutson et al. 2015; Sugi et al. 2017; Bacmeister et al. 2018; Wehner et al. 2018) and regional climate models (RCMs), with a focus on different ocean basins (Lavender and Walsh 2011; Knutson et al. 2013; Diro et al. 2014; Manganello et al. 2014; Jin et al. 2016; Wang et al. 2017). These studies have shown a wide range of basin-dependent potential shifts in future TC characteristics with respect to TC frequency

✉ José Abraham Torres-Alavez
jtorres@ictp.it

1 Earth System Physics, The Abdus Salam International Centre for Theoretical Physics (ICTP), Trieste, Italy

2 Climate Change Research Center, Institute of Atmospheric Physics, Chinese Academy of Sciences, Beijing, China

3 Department of Meteorology, University of Reading, Reading, UK

4 Computer Science and Engineering Division, Oak Ridge National Laboratory, Oak Ridge, TN, USA

5 Istituto di Oceanografia e di Geofisica Sperimentale (OGS), Trieste, Italy

of occurrence and the frequency of very intense TCs (Category 4–5). For both these variables, for example, there is no consistent signal of change across individual basins (Camargo 2013; Knutson et al. 2020), which might be related to differences in model resolution, physics, dynamical core or sea-surface temperatures (SSTs) warming patterns (e.g. Li et al. 2010; Walsh et al. 2010; Murakami et al. 2012b; Martínez-Sanchez and Cavazos 2014; Reed et al. 2015; Fuentes-Franco et al. 2017; Hsu et al. 2019).

The World Meteorological Organization (WMO) task team report (Knutson et al. 2010), the Fifth Assessment Report (AR5) of the Intergovernmental Panel on Climate Change (IPCC; Christensen et al. 2013), and Walsh et al. (2016) summarized the results of many modeling studies of future changes in TC climatology. They concluded that increasing greenhouse gas (GHG) concentrations is projected to lead to a global decrease in TC frequency by 5–30%, but with an increase in the frequency of TC categories 4 and 5 by up to 25%. They also reported an increase in TC lifetime and maximum intensity, along with increases in TC rainfall rate by 5–20%. However, these conclusions are highly basin- and scenario-dependent, and many uncertain aspects remain, such as the patterns of decrease in TC frequency, increase in very intense TCs (Category 4–5), and slowdown in TC translation speed (Knutson et al. 2020).

There is thus a need for further investigation of the TC's response to global warming, especially at the regional scale. This is particularly important in view of the fact that current GCMs used in the Coupled Model Intercomparison Project (CMIP) still suffer from the lack of sufficient model resolution to resolve important TC processes. One way to approach this issue is to use higher resolution RCMs (Murakami et al. 2012b; Giorgi 2019), which have demonstrated a relatively good performance in reproducing the general characteristics of TCs and have been used to assess the response of TC characteristics to global warming in different basins (e.g. Lavender and Walsh 2011; Knutson et al. 2013; Diro et al. 2014; Fuentes-Franco et al. 2017; Wang et al. 2017; Vishnu et al. 2019).

In this regard, recently a new set of twenty-first century projections with the RegCM4 regional model (Giorgi et al. 2012) have been completed for multiple domains defined by the COordinated Regional Downscaling EXperiment (CORDEX, Giorgi et al. 2009) as part of the CORDEX-CORE initiative (Gutowski et al. 2016). The simulations are conducted with 25 km grid spacing through downscaling of three GCMs from the CMIP5 ensemble (Taylor et al. 2012) for two GHG Representative Concentration Pathways (RCPs), the low end RCP2.6 and high end RCP8.5 (Moss et al. 2008). The availability of this new dataset thus offers the opportunity to analyze TC characteristics over multiple basins and their response to different global warming scenarios within a common simulation framework. The unique aspect of this analysis is that the different basins and scenarios are treated in a fully consistent way from a set of high-resolution RCM experiments following the same simulation protocol, which facilitates cross-basin and cross-scenario intercomparisons. In contrast, previous RCM-based work mostly focused on individual basins and/or scenarios.

We analyze a range of TC characteristics, such as frequency of occurrence, intensity, duration, track position, frequency of high intensity TCs, and precipitation associated with TCs. In addition, we analyze both the model performance in reproducing these characteristics under present day climate conditions, and the changes induced by global climate warming scenarios. In particular, we attempt to identify the physical mechanisms driving the simulated TC responses and discuss relevant underlying uncertainties.

The paper is organized as follows. The data, TC tracking algorithm and methods are first described in Sect. 2. Then, the evaluation of the model performance is presented in Sect. 3, while Sects. 4 and 5 examine the changes in tropical cyclone climatology and their driving mechanisms for the mid- (2041–2060) and late twenty-first century (2080–2099), under the RCP2.6 and RCP8.5 radiative forcing scenarios. A summary of the results, with final considerations, are finally given in Sect. 6.

2 Data and methods

2.1 Regional climate model

Here we analyze simulations with the RegCM version 4, or RegCM4, the latest version of the RCM developed by the Abdus Salam International Centre for Theoretical Physics (ICTP; Giorgi et al. 2012). RegCM4 utilizes the hydrostatic dynamical core from the mesoscale model MM5 (Grell et al. 1994), with split-explicit advection, sigma-p vertical coordinates and an Arakawa-b staggered horizontal grid. The model includes multiple physics options, and for each region, physics parameterizations were selected based on a series of preliminary experiments using boundary conditions from reanalyses aimed at optimizing the model performance over the different domains. This selection was not done specifically with the aim of TC simulation but for the CORDEX-CORE application as a whole and, as a standard procedure before use of RegCM4 for production runs, was based on standard metrics such as biases and probability density functions of variables such as temperature, precipitation and winds. For the Central America domain Diro et al. (2014) and Fuentes-Franco et al. (2017) have shown that the RegCM4 simulation of TC characteristics such as track density, frequency, lifetime and intensity is sensitive to the convection scheme and ocean flux parameterization used, and these studies have contributed to our choice of optimal

physics schemes for this domain. The schemes utilized for each domain are reported in Table 1.

The RegCM4 simulations follow the CORDEX-CORE protocol (Giorgi et al. 2012, Giorgi and Gutowsky 2015, Gutowski et al. 2016) over nine CORDEX domains (Giorgi et al. 2009). They extend from 1970 to 2099 with a horizontal grid spacing of 25 km and 23 vertical sigma levels. Three GCMs are downscaled for each of two RCPs, the low level RCP2.6 and the high-end RCP8.5 (Moss et al. 2008). Table 1 reports the driving GCMs used for each RegCM4 simulation (for the Northwest Pacific region only two simulations are currently available). These GCMs were chosen within the CORDEX-CORE protocol as performing generally well over the domains of interest (Elguindi et al. 2014) and having a low-, medium-, and high-equilibrium climate sensitivity (ECS), so as to approximately cover the CMIP5 climate sensitivity range.

The GCMs provide 6-hourly driving wind, pressure, temperature and water vapor as lateral boundary conditions for the RegCM4, and daily Sea Surface Temperature (SST) as lower boundary condition. In addition, the GHG concentrations in the RegCM4 are updated every 10 years based on observations for the historical period and on the selected scenario for the twenty-first century period, as is done in the driving GCMs.

Of the nine CORDEX-CORE domains, here we focus on five areas of TC formation each covered by a different domain (Fig. 2). We examine data for three 20-year periods, i.e. a reference historical period (1995–2014) and two future periods (2041–2060 and 2080–2099) for each scenario. Also, we compare the RegCM4 results with results from the driving GCMs, although due to the lack of some data for the RCP2.6 scenario, the GCM future runs are analyzed only for the RCP8.5. The TC characteristics analyzed, such as frequency, track density, intensity, lifetime and TC rainfall, are calculated for each simulation and each period separately. Then, ensemble averaged results are calculated by averaging of the individual simulations for each basin and period.

2.2 Data

To evaluate the simulated TCs, we use observed data from the International Best Track Archive for Climate Stewardship (IBTrACS, version v04; Knapp et al. 2010, 2018), which provides 6-h data of TC locations, surface wind speed and central pressure from different basins. IBTrACS collects observed TC data from 11 agencies around the world covering all major ocean basins where TCs occur: the North Atlantic (NA), Eastern Pacific (EP), western North Pacific (WP), North Indian Ocean (NI), South Indian Ocean (SI), and South Pacific (SP; Kruk et al. 2010). The minimum intensity reported by IBTrACS in each region varies from 25 kt (WP) to 30 kt (NA, EP) and 35 kt (NI, SI, SP), and here

Table 1 Details for models used in the simulations in each domain

Region	Driving GCMs	Physics scheme	Parametrization	References
Australasia		Boundary layer	Holtslag	Holtslag et al. (1990)
	HadGEM2-ES (Jones et al. 2011)	Cumulus (land)	Tiedtke	Tiedtke (1996)
	MPI-ESM-MR (Stevens et al. 2013)	Cumulus (ocean)	Tiedtke	Kain and Fritsch (1990), Kain (2004)
	NorESM1-M (Zhang et al. 2012)	Microphysics	SUBEX	Pal et al (2000)
		Ocean flux	Zeng et al.	Zeng et al (1998)
North Atlantic and Eastern Pacific		Boundary layer	Holtslag	
	HadGEM2-ES	Cumulus (land)	Emanuel	Emanuel (1991)
	MPI-ESM-MR	Cumulus (ocean)	Kain–Fritsch	
	GFDL-ESM2M (Dunne et al. 2012)	Microphysics	SUBEX	
		Ocean flux	Zeng et al	
North Indian		Boundary layer	UW PBL	Grenier and Bretherton (2001), Bretherton and Park (2009)
	MPI-ESM-MR	Cumulus (land)	Emanuel	
	NorESM1-M	Cumulus (ocean)	Tiedtke	
	MIROC5 (Watanabe et al. 2010)	Microphysics	SUBEX	
		Ocean flux	Zeng et al.	
Northwest Pacific		Boundary layer	Holtslag	
	MPI-ESM-MR	Cumulus (land)	Emanuel	
	NorESM1-M	Cumulus (ocean)	Emanuel	
		Microphysics	SUBEX	
		Ocean flux	Zeng et al.	

in order to facilitate a cross basin comparison we selected a common threshold of 17.5 m s^{-1} (~35 kt), which is used in the majority of the IBTrACS domains. Note that IBTrACS presents a homogeneous track dataset, with all non-10-min winds normalized to a 10-min average (Kruk et al. 2010).

For precipitation validation, we use the multi-source weighted-ensemble precipitation, version 2, (MSWEP-V2), a dataset based on a combination of rain-gauge measurements, satellite products and reanalysis data (Beck et al. 2017a, b). This dataset has shown good performance in describing precipitation over different regions around the world (Beck et al. 2017b, 2019; Liu et al. 2019; Satgé et al. 2020) and has been used in global TC precipitation studies (Zhang et al. 2019).

2.3 Cyclone tracking

Tropical cyclone tracking is based on the objective feature-tracking algorithm TRACK (Hodges 1994; 1995; 1999). This method has been widely used in previous studies for analyzing both tropical and extratropical cyclone tracks (Bengtsson et al. 2007, 2009; Manganello et al. 2012, 2014; Rastogi et al. 2018; Seiler et al. 2018). The algorithm initially identifies where grid point values of 6 hourly vertically averaged relative vorticity between 850 and 600 hPa are greater than 5×10^{-6} s^{-1} for the Northern Hemisphere (NH) and less than -5×10^{-6} s^{-1} for the Southern Hemisphere (SH)—at a spectral resolution of T63. These locations are refined using B-spline interpolation and greatest ascent maximization to find the off-grid maxima/minima. Initially, all systems are tracked by first initializing a set of tracks using a nearest neighbor method and then refining the tracks by minimizing a cost function for track smoothness. Following tracking, the T63 vorticity maxima/minima at all levels between 850 and 200 hPa (850, 700, 600,500, 400, 300, 200 hPa) are iteratively added to the tracks by searching for the extreme within a 5° radius (geodesic) of the cyclone centers. Additionally, the maximum 10-m wind within a 6° radius of the cyclone centers are added to the tracks. The TCs are initially identified from amongst all tracked features by applying criteria to detect a TC warm core, as a difference in the T63 vorticity field between 850 and 200 hPa greater than 6×10^{-5} s^{-1} and a vorticity maximum/minimum for all levels between 850 and 200 hPa for a coherent vertical structure and a maximum 10-m wind speed greater than 17.5 ms^{-1}. These criteria must be satisfied for at least one day over the oceans and the tracks must have lifetimes greater than 2 days. Furthermore, for this study the track lifecycles are restricted to where the maximum 10-m wind speed near the center of a cyclone is greater than 17.5 ms^{-1} during that part of the whole life cycle. For the GCMs, instead of using 10-m wind data, which are not available, following Franklin et al. (2003) and Walsh et al. (2007) we use the maximum 850 hPa wind speed near the center of the TC, with a threshold of 22 ms^{-1}.

2.4 Track density

The TC track density is defined for each 25 km grid point as the total number of days in a calendar year in which a storm center passes within a 500-km great circle distance of the grid point (Vecchi et al. 2014; Liu et al. 2018). The criteria for a 500-km storm size is used in observations and simulations and is consistent with previous TC studies (Chavas and Emanuel 2010; Barlow 2011; Prat and Nelson 2013; Khouakhi et al. 2017; and Liu et al. 2018).

2.5 TC intensity

At the present models' horizontal grid spacings (25 km for the RegCM4 and greater for the GCMs) it is impossible to reproduce observed cyclone wind intensities, which requires resolutions as fine as a few km (e.g. Gentry and Lackmann 2010). To overcome this systematic bias and adequately assess statistics of very intense tropical cyclones, the bias correction (BC) method used by Zhao and Held (2010) is applied to the simulated lifetime maximum 10-m wind speed (or 850 hPa wind for the GCMs). This method adjusts the wind speed of a simulated TC to the wind speed of the observed TC with the same probability in the cumulative distribution function of maximum wind speed. For each basin, the adjustment is calculated using observations from the IBTrACS dataset (Supplementary Figure S1). The BC method has some limitations that need to be considered when assessing TC intensities. First is the lack of a dynamical approach, which implies that non-linear responses are not accounted for and that the relationships yielding the BC must remain constant under climate change conditions. Second, the BC method needs sufficient information to provide a reliable result, i.e., the size of the TC sample could affect the results of the correction. Despite these shortcomings, the BC is probably the most reliable method to account for the drawback of insufficient model resolution and allow a consistent comparison of models with different resolutions, at least to a first order approximation (Zhao and Held 2010). Note that a comparison of observed TC intensities and RegCM4 results before the bias correction (Supplementary Figure S2) shows that the simulations reproduce, and in fact in some basins overestimate, TCs of intensity less than 50 ms^{-1} but underestimate the occurrence of the most intense TCs.

2.6 TC rainfall

Here the TC rainfall is defined as the rainfall within a 500-km radius of each TC center. Similar to Zappa et al. (2015) and Liu et al. (2018), the total annual accumulated

TC precipitation at a grid point can be expressed as $P = R \times F$, where P is the total storm rainfall, R is the average annual accumulated rainfall per storm, and F is the annual storm frequency expressed in days. Then, the change in rainfall related to TCs under GHG-induced warming can be directly attributed to the changes in the storm rainfall, or to the changes in storm frequency using $P' = R'F + RF' + R'F'$, where P' is the change of total storm rainfall, R' is the change in storm rainfall rate, and F' is the change in storm frequency. Therefore, the first and second terms are contributions from storm rainfall rate and frequency, respectively, while the third term is the covariance effect, generally much smaller than the other terms (Liu et al. 2018).

Additionally, similar to Khouakhi et al. (2017), we assess the changes in the contribution of TCs to extreme rainfall using the peak-over-threshold (POT) method. For the POT calculation, at each grid point we compute the number of days exceeding the 95th percentile for rainy days (i.e. days with precipitation > 1 mm), considering daily rainfall to be TC-induced only if the center of the storm is located within a 500-km radius of the grid point during a window of ± 1 day.

3 Assessment of model simulated TCs

Figure 1 shows the mean annual cycle of TC frequency for the IBTrACS observations, GCMs and GCM-driven RegCM4 simulations during the reference period for the five basins highlighted by the boxes in Fig. 2a. To determine the number of TCs in a particular month, we selected the time of maximum intensity in the simulations and IBTrACS. The observations show a peak of the TC season in August–September for the basins of the Northwest and Eastern Pacific and North Atlantic Ocean, a double peak in the North Indian Ocean and a maximum in January through March over Australasia. The timing of seasonal peaks in TC activity are mostly reproduced by the RegCM4 simulations, although in some cases discrepancies of one month are found in the timing of the peak. Specifically, for the Northwest Pacific and North Atlantic basins the peak is shifted to September–October, while for the Eastern Pacific to July–August. These shifts mostly follow corresponding shifts in the driving GCMs, except over the Eastern Pacific. In addition, for the North Indian Ocean (Fig. 1d), the RegCM4 simulations

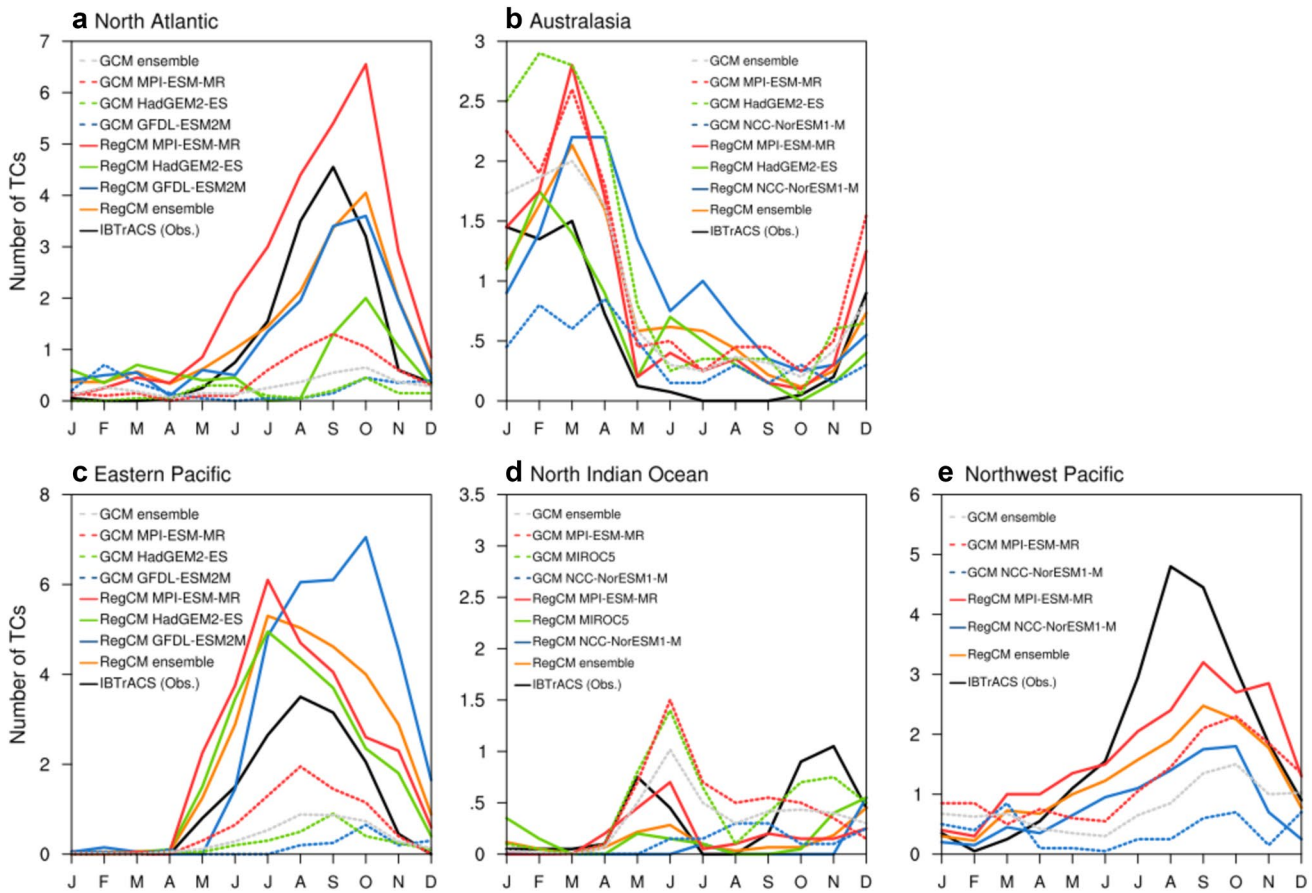

Fig. 1 TC annual cycle over **a** the North Atlantic Ocean, **b** Australasia, **c** the Eastern Pacific Ocean, **d** the North Indian Ocean and **e** the Northwest Pacific Ocean during 1995–2014

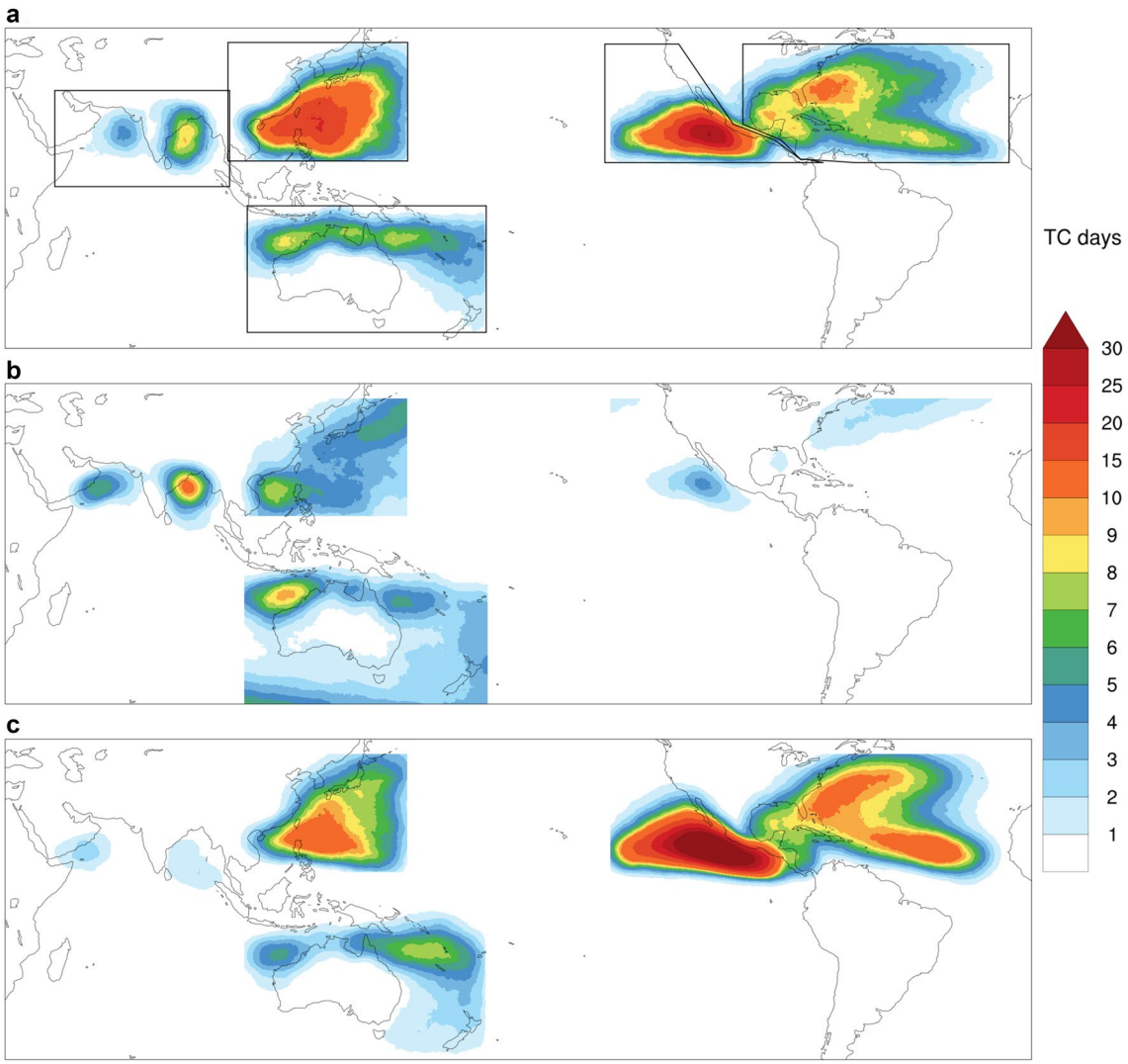

Fig. 2 TC track density (TC days in a calendar year in which a storm center passes within a 500-km great circle distance of a grid point) for 1995–2014 from **a** IBTrACS, **b** GCM ensemble mean and **c** RegCM4 ensemble mean

Table 2 Correlation coefficients between model and observed TC annual cycle (*R*) and their mean absolute error (MAE)

	North Atlantic		Australasia		Eastern Pacific		North Indian		Northwestern Pacific	
	R	MAE	R	MAE	R	MAE	R	MAE	R	MAE
GCM ensemble	0.81	1.04	0.94	0.35	0.95	0.88	0.44	0.27	0.55	1.28
GCM HadGEM2-ES	0.36	1.10	0.91	0.66	0.86	0.97				
GCM MPI-ESM-MR	0.95	0.84	0.97	0.55	0.99	0.57	0.28	0.35	0.68	1.01
GCM NorESM1-M			0.67	0.38			−0.04	0.32	−0.03	1.62
GCM MIROC5							0.63	0.22		
GCM GFDL-ESM2M	−0.22	1.22			0.28	1.11				
RegCM4 ensemble	0.88	0.6	0.85	0.38	0.94	1.08	0.42	0.23	0.91	0.71
RegCM4 HadGEM2-ES	0.41	1.04	0.84	0.27	0.93	0.72				
RegCM4 MPI-ESM-MR	0.92	1.03	0.92	0.36	0.9	1.03	0.42	0.23	0.86	0.68
RegCM4 NorESM1-M			0.56	0.61			0.04	0.31	0.91	1.06
RegCM4 MIROC5							0.39	0.27		
RegCM4 GFDL-ESM2M	0.89	0.57			0.82	1.63				

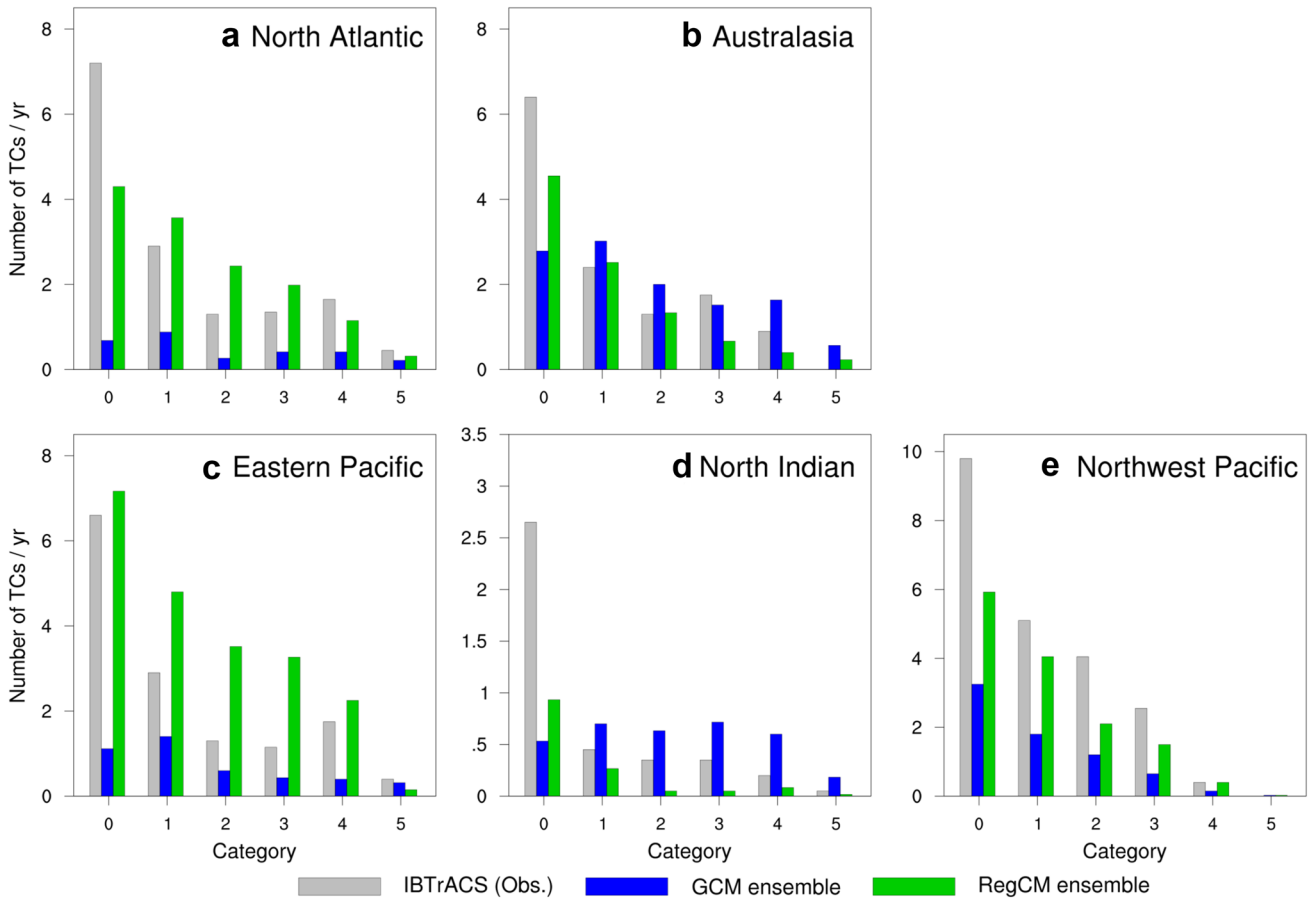

Fig. 3 Annual number of TCs categorized by the Saffir-Simpson scale (after bias correction) for **a** the North Atlantic Ocean, **b** Australasia, **c** the Eastern Pacific Ocean, **d** the North Indian Ocean and **e** the Northwest Pacific Ocean for 1995–2014. Category 0 refers to storms of Tropical Storm intensity

are not capable of producing the second maximum of TC activity, which is better captured by the MIROC5 GCM. In the other cases, the GCMs tend to severely underestimate the TC occurrence, except for the MPI-ESM-MR and HadGEM2-ES models over Australasia. In the other basins, the RegCM4 simulations produce an annual TC frequency closer to the observed (IBTrACS) when compared with the GCMs.

Considering the ensemble average, the RegCM4 simulations tend to overestimate the TC frequency over the Eastern Pacific and Australasia, and to underestimate it over the Northwest Pacific and North Indian Ocean. The model performance is poorest over the North Indian Ocean (except for the MPI-ESM-MR -driven runs), with the GCMs producing more TCs. Importantly, in most cases the RegCM4 ensemble mean appears more consistent with IBTrACS than the individual RegCM4 simulations, demonstrating the general usefulness of the ensemble and its better reliability for this analysis.

For a quantitative assessment of the model in reproducing the TC frequency, Table 2 shows the correlation coefficients between the simulated (individual and ensemble GCMs and RCMs) and observed (IBTrACS) annual cycle of TC frequency for each basin, along with the mean annual absolute error (MAE) calculated as the sum of the monthly MAE. For four of the five basins in RegCM4, (except the North Indian Ocean) and three basins in the GCMs (except the North Indian Ocean and the Northwestern Pacific), the correlations are quite high, demonstrating a good performance by the individual simulations and the ensembles. The ensembles mostly show intermediate MAE in comparison with the individual simulations, and in comparison with the GCMs, the RegCM4 simulations show a better MAE over the North Atlantic and Northwestern Pacific oceans. For the other basins the differences in correlation and MAE across the two sets of models are small.

The geographic distribution of the TC track density for IBTrACS, GCM and RegCM4 simulations are shown in Fig. 2a–c, respectively. The observed track density shows maxima in TC activity over the Northwest Pacific, tropical eastern Pacific, the ocean areas off the eastern coast of the United States, the Gulf of Mexico, the Bay of Bengal, and

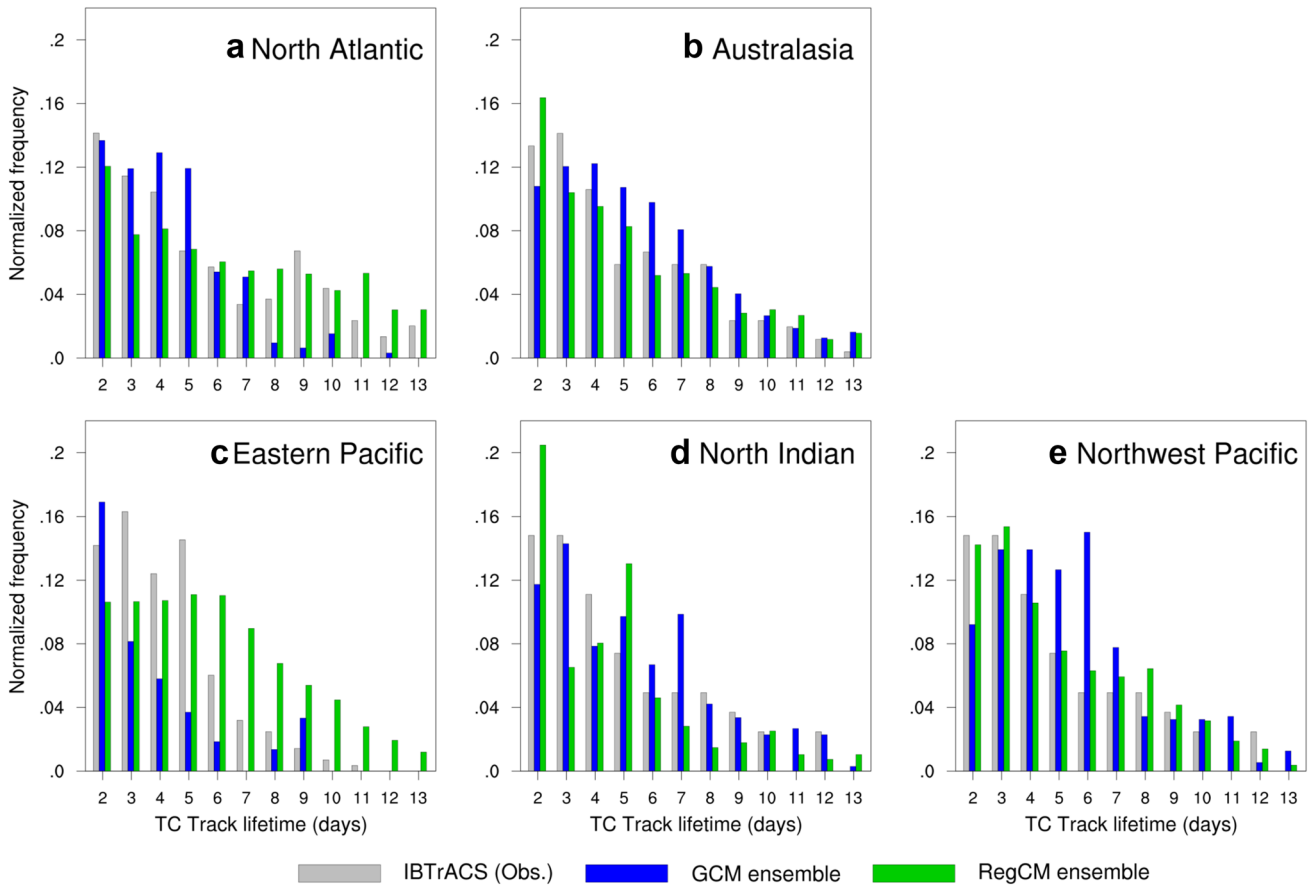

Fig. 4 Normalized frequency (by the total number of TCs for each respective simulation and basin) of TC track lifetime for **a** the North Atlantic Ocean, **b** Australasia, **c** the Eastern Pacific Ocean, **d** the North Indian Ocean and **e** the Northwest Pacific Ocean for 1995–2014

Table 3 Correlation coefficients between model and observed life cycle (normalized frequency) of TC (*R*) and their mean absolute error (MAE)

	North Atlantic		Australasia		Eastern Pacific		North Indian		Northwestern Pacific	
	R	MAE	R	MAE	R	MAE	R	MAE	R	MAE
GCM ensemble	0.83	0.025	0.89	0.017	0.63	0.042	0.85	0.020	0.65	0.032
RegCM4 ensemble	0.95	0.017	0.92	0.016	0.75	0.037	0.86	0.028	0.97	0.010

the tropical regions of Australia and adjacent oceans. The ensemble of GCMs is not able to reproduce the regions of maximum TC activity over the Northwest Pacific, tropical eastern Pacific and North Atlantic and overestimates the TC density over the Bay of Bengal and northwestern Australia.

The RegCM4 captures the spatial patterns of the TC climatology such as the maximum concentration over the tropical Eastern and Western Pacific, the western Atlantic, and northern Australia. The main model deficiency is the underestimation of TCs over the two cyclogenetic areas of the Indian Ocean, the Bay of Bengal and the Arabian Sea, areas where problems have been encountered also in previous studies using GCMs and RCMs (Manganello et al. 2012; Knutson et al. 2015; Bacmeister et al. 2018; Vishnu et al. 2019). The poor results in simulating TCs over the North Indian Ocean could be related to the difficulty in separating monsoon depressions from TCs in our tracking criteria and to a cold bias in sea surface temperature (SST) simulated over the North Indian Ocean in the GCMs (Supplementary Figure S3). Overall, Fig. 2 shows that, compared to the GCMs, the RegCM4 simulates TC patterns which are closer to observations except for the two TC areas in the North Indian Ocean.

To investigate the physical processes underlying the TC frequency bias described in the GCMs above, we examine the bias (model minus ERA5 reanalysis) in SST, relative humidity at 700 hPa (RH700) and vertical wind shear (Vs) for the GCMs (Supplementary Figure S3). The

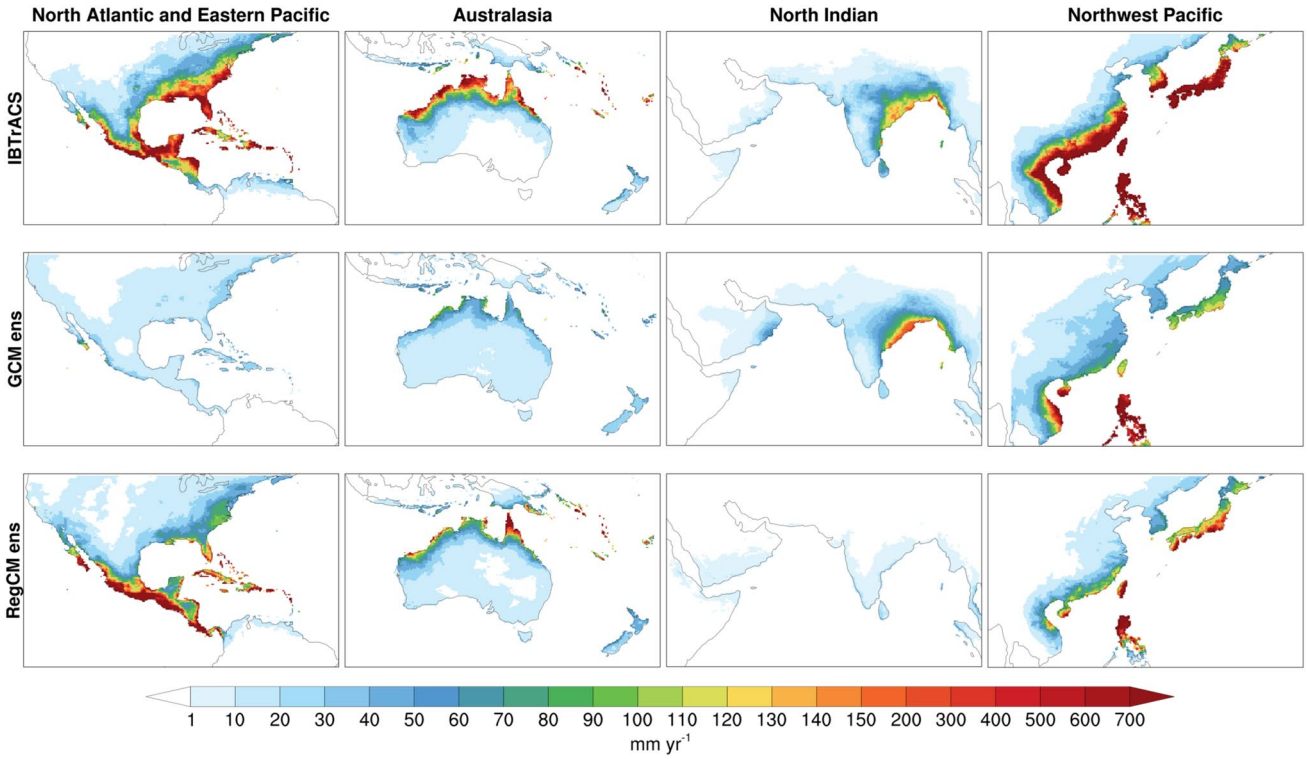

Fig. 5 Spatial distribution of the mean annual TC rainfall (mm year^{-1}) for (left)–(right) the North Atlantic Ocean, Eastern Pacific Ocean, Australasia, North Indian Ocean and Northwest Pacific Ocean, (top)–(bottom) from IBTrACS with MSWEP precipitation, GCM ensemble mean and RegCM4 ensemble mean

Table 4 Pattern correlations coefficients between model and observed TC rainfall (R) and their mean absolute error (MAE, mm year^{-1})

	North Atlantic		Australasia		Eastern Pacific		North Indian		Northwestern Pacific	
	R	MAE	R	MAE	R	MAE	R	MAE	R	MAE
GCM ensemble	0.81	16.2	0.89	14.4	0.64	6.9	0.92	6.8	0.83	31
RegCM4 ensemble	0.85	11	0.83	10.9	0.86	7.6	0.37	16	0.91	32.5

underestimation in North Atlantic storms in the three GCMs can be potentially explained by the cold SST and dry RH700 biases in two of the models. Furthermore, the North Atlantic tropical cyclone genesis is strongly linked with tropical easterly waves, and these waves are not well represented in the GCMs (Camargo 2013). Similarly, the low production of TCs in the NorESM1-M model over Australasia, Northwestern Pacific and North Indian Ocean could be related to a cold SST bias there. The MPI-ESM-MR is the model with the smallest bias in SST and RH700 and storm simulations in this model are closer to observations in all domains.

Figure 3 shows the mean annual TC frequency on the Saffir–Simpson hurricane wind scale after the wind adjustment is carried out for both model ensembles. For the North Atlantic, Australasia and Northwest Pacific (Fig. 3a, b, e), the RegCM4 experiments in each category are in line with the observations except for a systematic underestimation of tropical storms (Category 0). For the Eastern Pacific, the RegCM4 ensemble mean overestimates TCs in all categories, except Category 5, while over the North Indian Ocean (Fig. 3d), as already discussed, the RegCM4 ensemble simulations produce too few TCs. The GCM ensemble severely underestimates TCs in all categories for the North Atlantic, Eastern Pacific and Northwest Pacific basin, and it overestimates TCs over the North Indian Ocean basin (except for Category 0) and is comparable to observations over Australasia (again except for category 0). Overall, the models

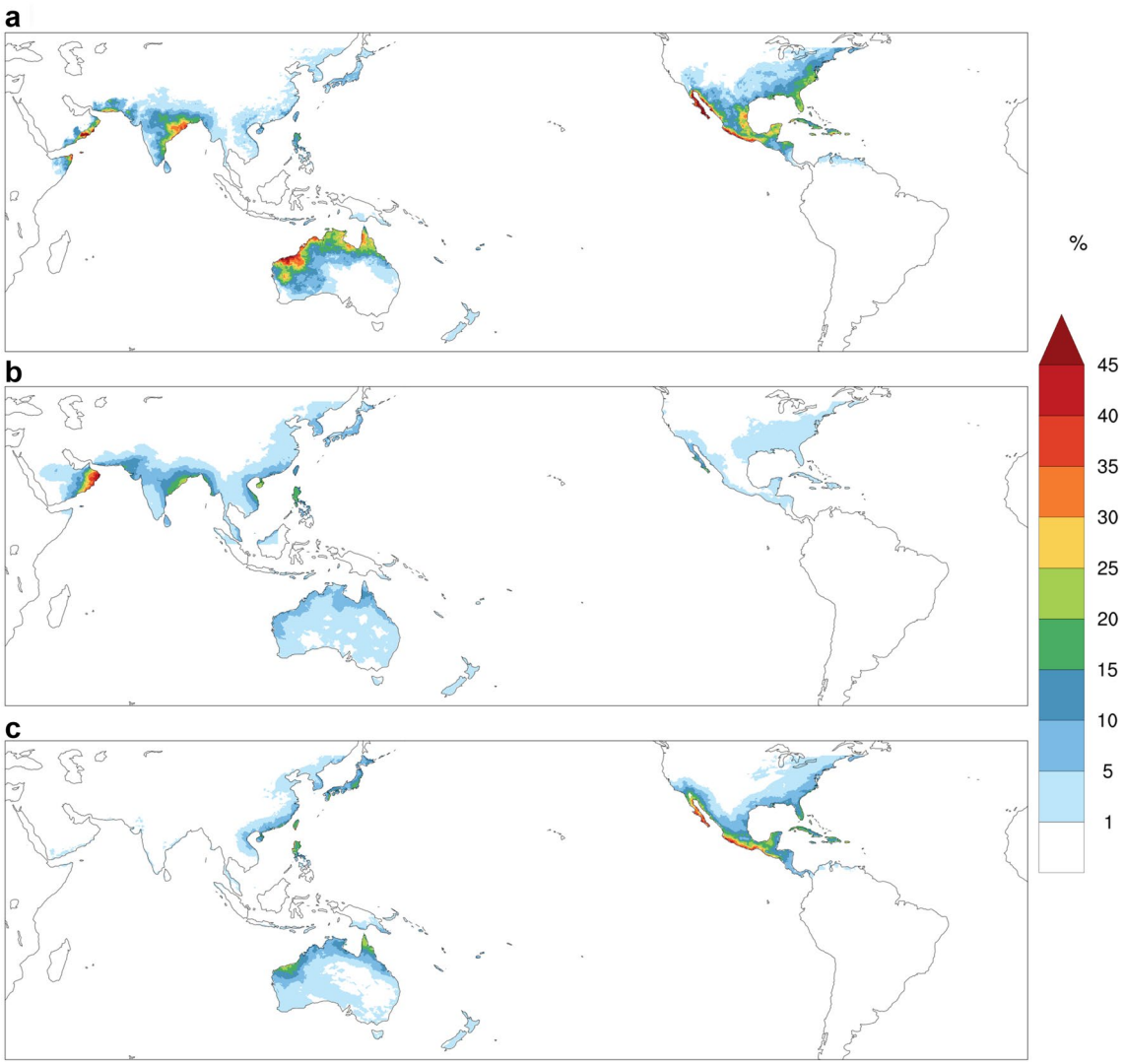

Fig. 6 Relative contribution of TCs to extreme rainfall using the POT approach (%) for 1995–2014 from **a** IBTrACS with MSWEP precipitation, **b** GCM ensemble mean and **c** RegCM4 ensemble mean

Table 5 Pattern correlations coefficients between model and observed contribution of TCs to extremes of precipitation (*R*) and their mean absolute error (MAE; %)

	North Atlantic		Australasia		Eastern Pacific		North Indian		Northwestern Pacific	
	R	MAE	R	MAE	R	MAE	R	MAE	R	MAE
GCM ens	0.79	3	0.86	6	0.83	2	0.75	3	0.84	1
RegCM ens	0.9	2	0.9	4	0.88	1	0.44	5	0.83	1

tend to systematically underestimate category 0 events and to show more mixed results for the other categories.

Figure 4 shows the storm duration in each basin. Overall, the RegCM4 experiments simulate adequately the lifetime of the events and improve those generated by the GCMs over Australasia, the Northwest Pacific and North Atlantic Ocean, as measured by the higher values of correlation (Table 3) for the RegCM4 ensembles (> 0.92) compared to those in the GCM ensembles (> 0.65) in all basins. For the North Indian Ocean, the GCMs better simulate the long-lived events (Fig. 4d) and also exhibit a lower MAE than the RegCM4. In the Eastern Pacific (Fig. 4c), neither the GCMs (underestimate) nor the RegCM4 (overestimate) can reproduce adequately the duration of the TCs, presenting relatively low correlations and high MAEs.

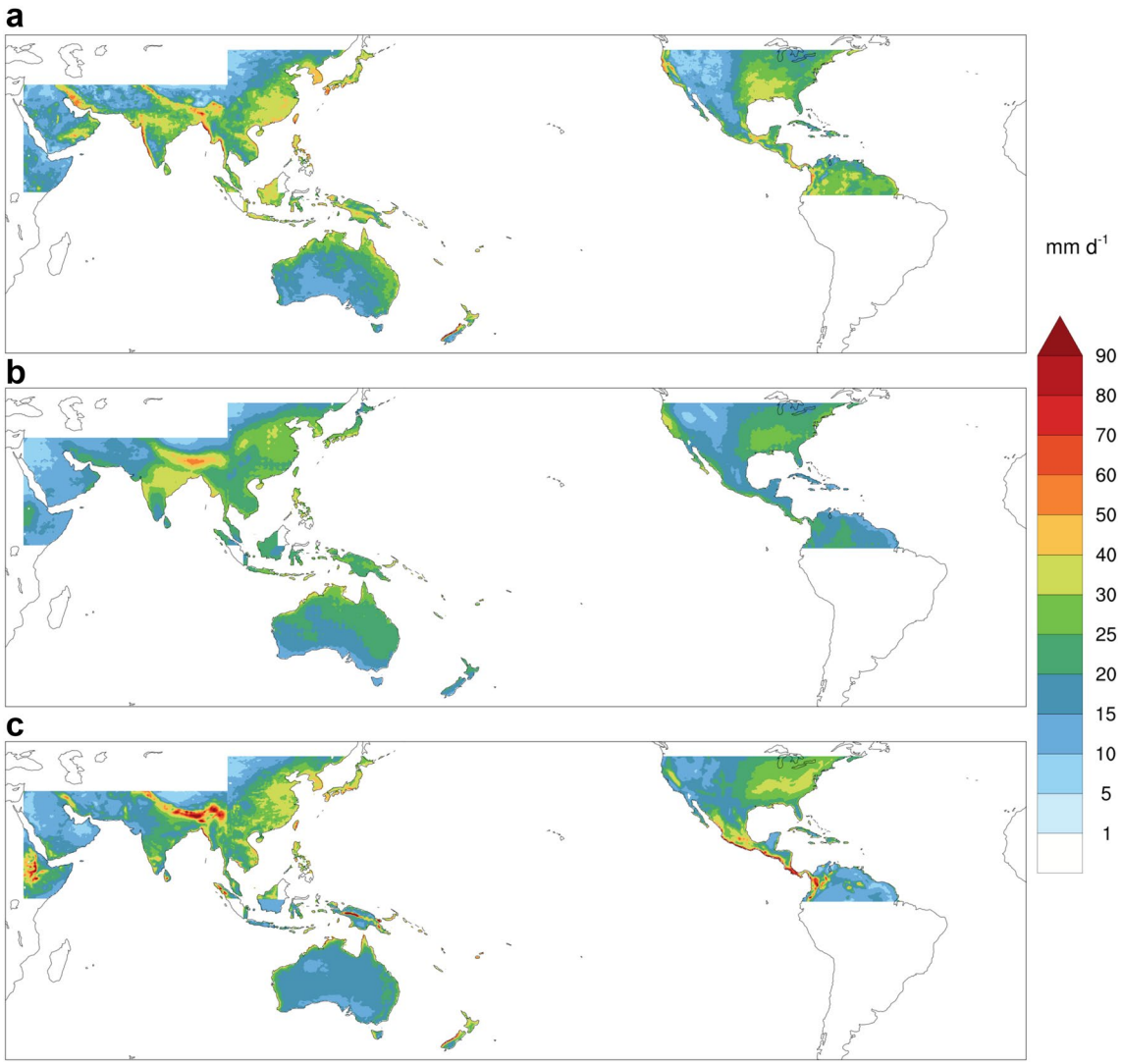

Fig. 7 95th percentile of precipitation (mm day^{-1}) for 1995–2014 from **a** IBTrACS with MSWEP precipitation, **b** GCM ensemble mean and **c** RegCM4 ensemble mean

The average annual rainfall associated with TCs is displayed in Fig. 5. The observed climatology of TC rainfall (MSWEP) has the largest magnitude in the eastern United States, southern Mexico, eastern China, Japan, northern Australia, eastern India and Bangladesh (Fig. 5 top panels). This is supported by a higher TC density in these regions (Fig. 2). The GCM ensemble (Fig. 5 middle panels) shows good agreement with observations over the coasts of the Bay of Bengal and the South China Sea, with correlations of 0.92 over the North India Ocean (Table 4); but there is a large underestimation of TC precipitation over the other regions. The RegCM4 ensemble (Fig. 5 bottom panels) is generally closer to observations than the GCMs over the coastal regions of central and south America, Australia and northeastern Asia, reaching values of correlation higher than 0.83 (Table 4) and lower MAE over Australasia and North Atlantic. However, it substantially underestimates TC precipitation over the Bay of Bengal and Vietnam coasts.

To quantify the relevance of cyclones for extreme precipitation events, we examined the TC impact on extreme rainfall using the POT approach. Using the TC tracks from IBTrACS and the MSWEP precipitation (Fig. 6a), we find that Baja California and the Pacific Coast of southwestern Mexico are the most affected by TC-induced heavy rainfall, where more than 45% of the 95th percentile rainfall is TC-related. Other regions such as northwestern Australia, eastern India, the southern part of the Arabian Peninsula, and Somalia (Fig. 6a) show a large contribution from TC-induced heavy rainfall, while in the southeastern United States and the Caribbean region, values are in the range of 15% to more than 25% in the Yucatan Peninsula.

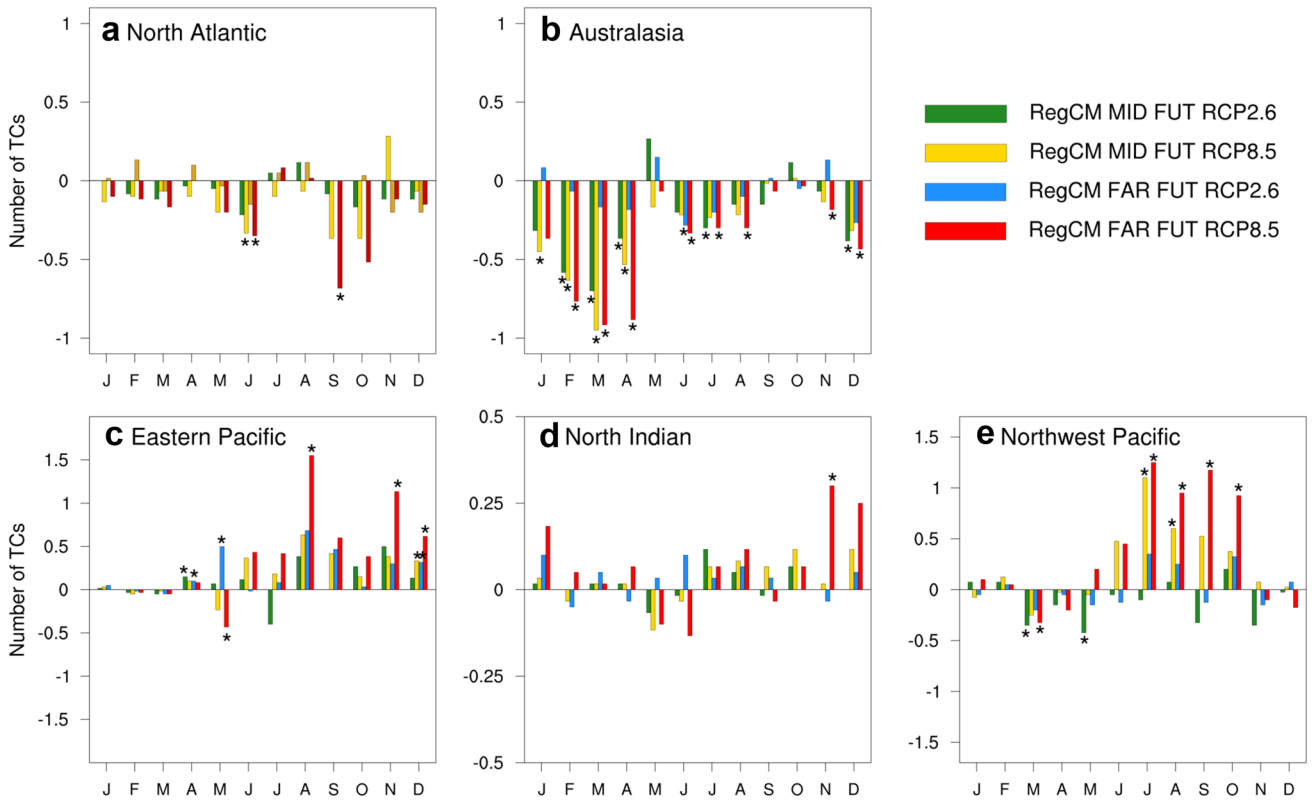

Fig. 8 Changes in TC annual cycles for the RegCM4 for **a** the North Atlantic Ocean, **b** Australasia, **c** the Eastern Pacific Ocean, **d** the North Indian Ocean and **e** the Northwest Pacific Ocean. The mid-future period refers to 2041–2060 and the far-future period refers to 2080–2099. Asterisks show where changes are significant to a 95% level of confidence, based on the Wilcoxon rank-sum test

In general, the GCMs underestimate the contribution of TCs to extremes of precipitation over northern Australia, North and Central America (Fig. 6b, Supplementary Figure S4a), with MAE between 2–6% in the basins of North Atlantic, Eastern Pacific and Australasia (Table 5), and overestimate it over eastern Asia. They do, however, capture adequately the spatial pattern over Japan. Similar to the results for total precipitation (Fig. 5c), the RegCM4 simulations (Fig. 6c, Supplementary Figure S4c) underestimate the TC contribution to extreme rainfall over the North Indian Ocean and Australia (MAE between 4 and 5%, Table 5). However, the ensemble mean shows only a small underestimation along the southwestern Mexican coast and the northern coasts of Australia, with high values of correlation (0.9) and low MAE (Table 5) over Australasia and the North Atlantic Ocean, improving the GCMs results there. The general underestimation of TC-induced precipitation can probably be attributed to the relatively low track density in the RegCM4 simulations compared with observations over coastal areas (Fig. 2).

The spatial distribution of 95th-percentile precipitation (RR95p), as obtained from the MSWEP observations and the GCM and RegCM4 ensembles, is presented in Fig. 7. In the observed field (MSWEP, Fig. 7a), the highest values of 95th-percentile precipitation (RR95p) appear over the Himalayan foothills, the western Indochina Peninsula, western India and southern Japan. Both the GCMs and RegCM4 capture the main observed features of RR95p. However, the GCMs (Fig. 7b, Supplementary Figure S4b) show a larger bias over eastern Asia, and an overestimation over Australia and India, while the RegCM4 simulations (Fig. 7c, Supplementary Figure S4d) show an overestimation in the Himalayas, Mexico and Central America and an underestimation over Australia and India.

In summary, the RegCM4 ensemble shows a relatively good performance in reproducing most of the observed TC characteristics over the different basins analyzed, in several regions improving the driving GCM results. The exception is the North Indian Ocean basin, where the regional model underestimates TC occurrences and the GCM ensemble actually produces a better TC climatology, especially in the second peak of the TC season.

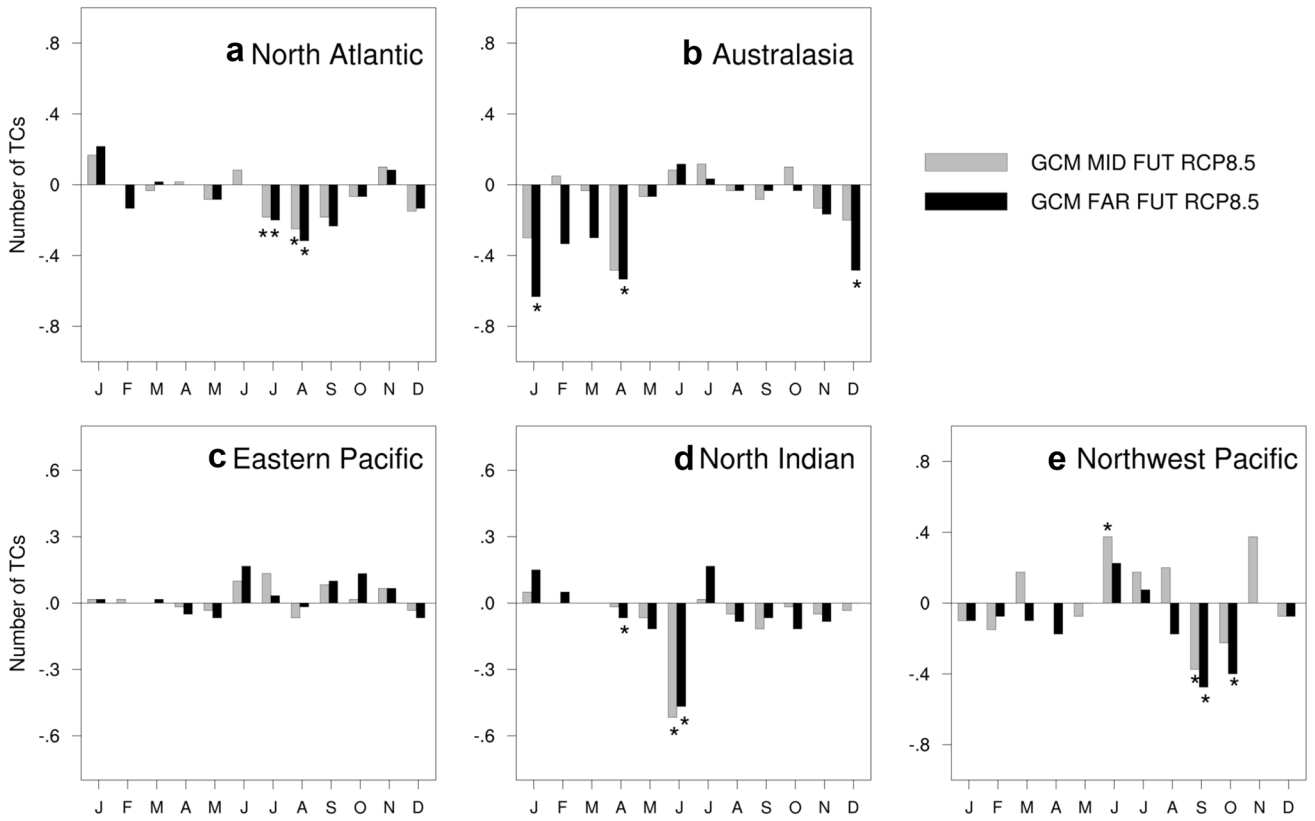

Fig. 9 As in Fig. 8, but for the GCMs under the RCP8.5 scenario

4 Future projections of TC characteristics

In this section, we examine the changes in TC characteristics for the mid- (2041–2060) and late (2080–2099) twenty-first century time slices relative to the baseline period (1995–2014) under the RCP8.5 and RCP2.6 scenarios.

The projected changes in the TC seasonal cycle from the RegCM4 ensemble mean are shown in Fig. 8. For the North Atlantic (Fig. 8a) and Australasia (Fig. 8b), the simulations project a prevailing decrease in TC occurrence, especially during the climatologically active TC months (June to September in the Atlantic and February to April in Australasia). For the RCP8.5 and the late future, the changes are statistically significant at the 95% confidence level, reaching a decrease in the North Atlantic of − 2.3 and in Australasia of − 4.6 TCs per year. For the Eastern Pacific (Fig. 8c), North Indian Ocean (Fig. 8d) and Northwest Pacific (Fig. 8e), the models show opposite trends, with a prevailing increase in TC frequency, especially for the far future RCP8.5 (4.7, 0.85 and 4.3 TCs per year, respectively). More specifically, we find a significant increase in TC activity in the Eastern Pacific during April, August, November and December under the RCP8.5 scenario, thus leading to a longer TC season, running from April to December (instead of May to November for present day conditions). For the North Indian Ocean, the largest and most significant changes occur in November and December, during the second peak of TC activity. For the Northwest Pacific, the increase is found during the peak of the season (July–October). Overall, our projected changes in the frequency of TCs are qualitatively consistent with the changes found in the CMIP3 models (Knutson et al. 2010) and with the CMIP5-RCP4.5 scenario (Knutson et al. 2015). Interestingly, the changes over the North Indian Ocean and North Atlantic Ocean for the latter part of twenty-first century and the low-emissions scenario are larger than those reported for the same period by Knutson et al. (2015). The discrepancy among different results may partly be explained by differences in the design of the experiments, tracking algorithms and subsets of CMIP5 models included in the studies.

The changes in the TC seasonal cycle from the GCMs (Fig. 9) are generally similar to those in the RegCM4 over the Eastern Pacific, North Atlantic and Australasia, but of smaller magnitude. Conversely, for the North Indian and Northwest Pacific Ocean, the GCMs project a decrease in the number of TCs during the peak season, opposite to those projected in the RegCM4 simulations.

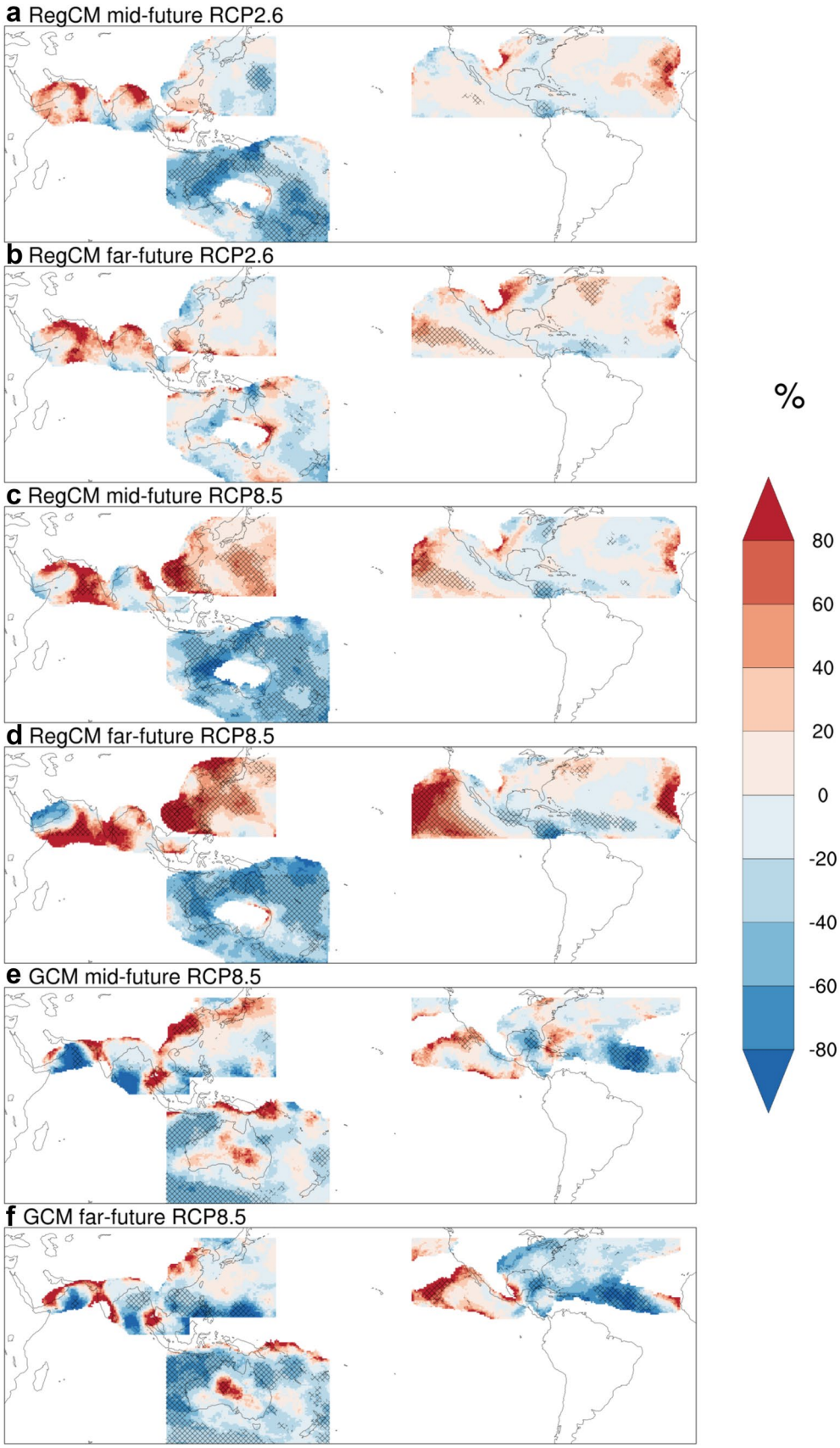

◂**Fig. 10** Percent change in TC track density relative to the baseline period for the RegCM4 ensemble mean under the RCP2.6 scenario for the **a** mid- and **b** far-future; under the RCP8.5 scenario for the **c** mid- and **d** far-future and for the GCM ensemble **e** mid- and **f** far-future. The mid-future period refers to 2041–2060 and the far-future period refers to 2080–2099. The map shows regions with a track density of least 5 days in the historical period. Hatched areas show where changes are significant to a 95% level of confidence, based on the Wilcoxon ranksum test

Figure 10 shows projected ensemble-mean changes in the spatial distributions of TC occurrences as percentage change relative to the baseline period (1995–2014). Hatched areas indicate where these changes are statistically significant at the 95% confidence level. For the RCP8.5 scenario, the track densities in the RegCM4 experiments show consistent changes in the two time slices, with greater magnitudes in the far future one: a strong and statistically significant decrease over the Australasia region; a strong and statistically significant increase in the northwestern Pacific; in the eastern Arabian Sea and, in the far future period, over the Bay of Bengal; a prevailing decrease over the Gulf of Mexico, with an increase north of these regions over the ocean areas off the coasts of the United States; a decrease over the eastern Pacific coastal regions, with an increase further west over the ocean. These results are consistent with those reported by Murakami et al. (2013, 2017) for the North Indian Ocean and Gleixner et al. (2014) for Australasia (about +40 and −20%, respectively).

Some of these patterns are similar in the RCP2.6, but with more mixed features. It is interesting to note for RCP2.6 in the mid-future period (Fig. 10a) the changes are more pronounced than by the end of the century (Fig. 10b). This could be explained by the fact that the radiative forcing for the RCP2.6 scenario reaches its peak by mid-century and after that, it slightly declines toward the end of the century.

The results over the North Atlantic and Eastern Pacific mostly agree with previous simulations by Diro et al. (2014) and Knutson et al. (2015), with the exception of the northwestern part of the North Atlantic Ocean. Over this region, Knutson et al. (2015) found a decrease in TC frequency, in contrast to the increase shown in our results and in previous studies using a downscaling framework with CMIP3 (Emanuel et al. 2008) and with CMIP5 data (Diro et al. 2014). Note that aside from the Australasia and Gulf of Mexico regions, the GCMs show patterns which are quite different from those of the RegCM4, often in fact of opposite sign, such as over the Bay of Bengal and the South China Sea.

Concerning landfalls, we find in the RegCM4, RCP8.5 scenario, significant and robust increases over the land surfaces bordering the South China Sea, such as Vietnam, southern China and for the far future the Philippines, where populations are already vulnerable to TC-induced flooding (Gupta 2010). In addition, in the late twenty-first century RCP8.5 there is a significant increase in TC density over the offshore areas northeast of the United States, indicating a greater potential for damage in this region, although a decrease is found over the Eastern US in the mid-future slice.

Another important feature to consider is the impact of climate change on TC intensity. The changes in the ensemble mean annual TC frequency on the Saffir-Simpson Scale are shown in Fig. 11. In general, the GCM and RegCM4 bias-adjusted model output shows either small or positive changes in the frequency of more intense (Categories 4 and 5) TCs in all basins, with prevailing positive changes in the RCP8.5 scenario, by 1.2, 3, 0.3 and 0.6 TCs year^{-1} over the North Atlantic, Eastern Pacific, North Indian Ocean and Northwest Pacific basins respectively. Over Australasia and the North Atlantic basin, the number of low-intensity TCs (Categories 0–2) are significantly reduced in both ensembles in the RCP8.5, while for the Eastern Pacific an increase in TCs is projected for all categories. Over the North Indian Ocean we find the largest disagreement between RegCM4 and GCM projections, with opposite signs of changes between the ensembles, while finally a generally mixed change response is seen in the Northwest Pacific. In general, the results using winds without bias correction are in line with the bias corrected ones (Supplementary Figure S5).

The increase in the occurrence of high-intensity TCs is consistent with Knutson et al. (2015), who also project a large increase in TCs of categories 4–5 for the Eastern Pacific, North Atlantic, Northwest Pacific and Arabian Sea, by the end of the twenty-first century. However, the RegCM4 results are opposite to those of Knutson et al. (2015) over the northeastern Indian Ocean, where they report a decrease. These differences may be related to the different model resolutions and simulation design, although we emphasize that the North Indian Ocean is the region where the RegCM4 simulated TC statistics show the lowest performance with respect to observations.

Figure 12 shows the RegCM4 ensemble-mean projected changes in TC duration, where the values of TC duration are normalized with respect to the total number of TCs in each period. Three of the five domains (North Atlantic, Australasia and Northwest Pacific) show a reduction in the number of TCs with a long life cycle, especially those lasting longer than seven days, while the North Indian Ocean basin shows small changes and the Eastern Pacific an increase in correspondence with a consistent reduction in the frequency of short-duration TCs. The results for this latter basin are qualitatively in agreement with those of Emanuel et al. (2008). For the other basins, the response of short-duration events shows mixed signals. The changes in TC duration projected by the GCMs (Supplementary Figure S6) show more mixed results, but of relevance is the fact that the GCM-produced

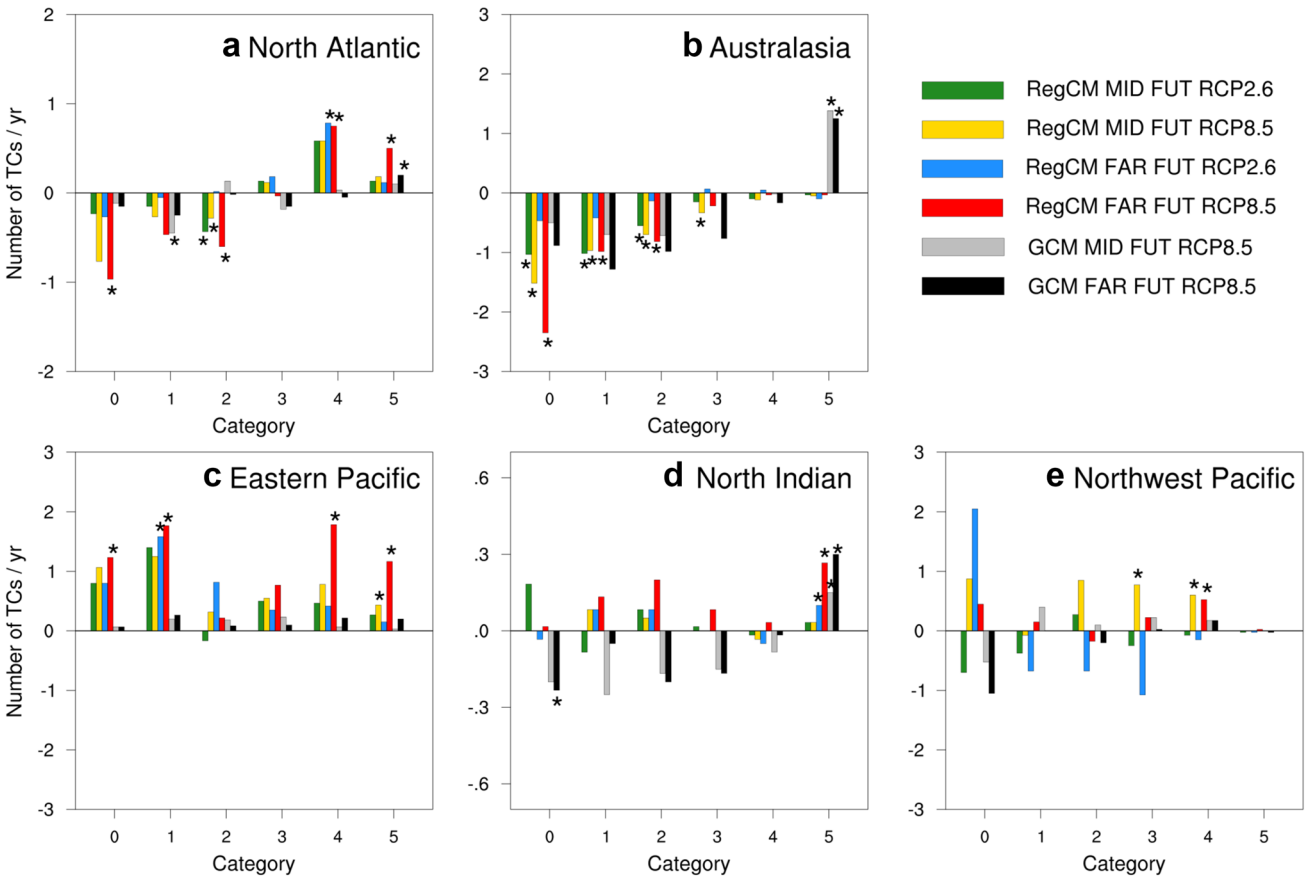

Fig. 11 Changes in the annual number of TCs as categorized by the Saffir-Simpson scale (after bias correction) for **a** the North Atlantic Ocean, **b** Australasia, **c** the Eastern Pacific Ocean, **d** the North Indian Ocean and **e** the Northwest Pacific Ocean. The mid-future period refers to 2041–2060 and the far-future period refers to 2080–2099. Asterisks show where changes are significant to a 95% level of confidence, based on the Wilcoxon rank-sum test

responses are of opposite sign compared to the RegCM4s over the Australasia and Eastern Pacific Basin.

Figure 13 shows the change of mean annual TC rainfall in the different periods and scenarios for both the RegCM4 and GCM ensembles. In the RegCM4, under both scenarios, we find a significant decrease over Australasia (hatched areas), by up to 60–90%, and over Mexico and Central America by 20–40%, except for areas of northern Mexico. Over India, the Arabian Peninsula, Myanmar, eastern China and Japan, the RCP8.5 RegCM4 projections show large increases, significant in some regions, although this signal reverses sign in RCP2.6 in some areas of southeastern China and northern Indochina Peninsula. The eastern coastal regions of the United States show different changes depending on the forcing and period analyzed. Moving to the GCM projections, in several cases changes are of opposite sign between the GCMs and RegCM4, most noticeably over Australasia and southern Mexico.

Turning our attention to the changes in the TC contribution to extreme precipitation (Fig. 14), in the RegCM4, consistent with the differences in the rainfall rate, for all future periods and scenarios, the percentage of extremes related to TCs primarily increases over the North Indian Ocean, eastern China, Korea, and Japan by 20%. Over northern Australia, Mexico and the eastern United States, our simulations indicate a prevailing, but not ubiquitous, decrease in the percentage of high-precipitation events related to TCs, the change being larger for the RCP8.5 and for the late future. Observational studies (Cavazos et al. 2008; Pfahl and Wernli 2012) are consistent with these trends in the future projections. Again, the GCMs show some instances of noticeably different responses, such as over Australasia and Mexico.

5 Analysis of driving mechanisms

The occurrence and development of TCs depends strongly on the SSTs and on characteristics of the large-scale environment such as vertical wind shear (Vs) and vertical

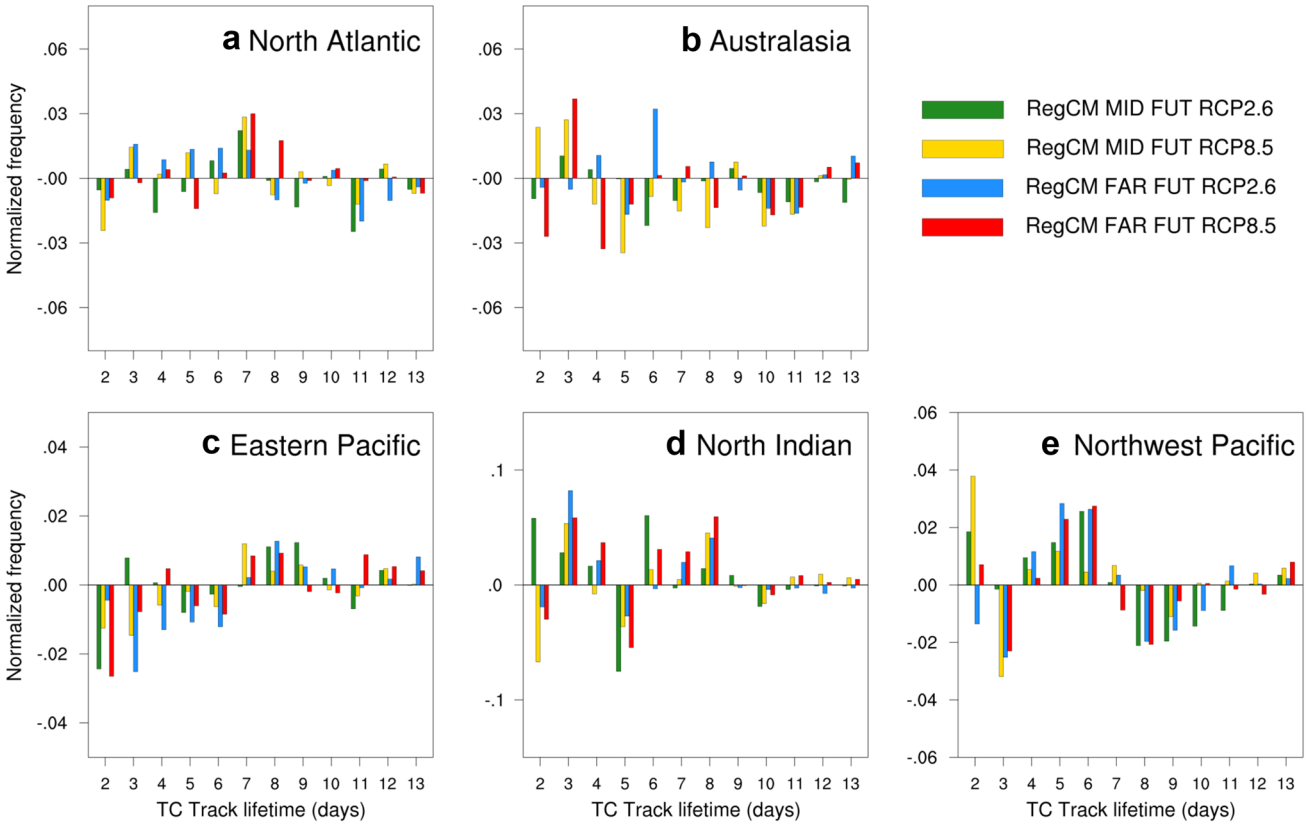

Fig. 12 Normalized changes (by the total number of TCs for each respective simulation and basin) in the TC track lifetime for the RegCM4 for **a** the North Atlantic Ocean, **b** Australasia, **c** the Eastern Pacific Ocean, **d** the North Indian Ocean and **e** the Northwest Pacific Ocean. The mid-future period refers to 2041–2060 and the far-future period refers to 2080–2099

thermodynamic profiles (Emanuel 1995). In general, the SST increases in the future, which should lead to increased TC occurrence and intensity. However, other atmospheric factors can drastically modulate this response and can help to explain the strongly basin-dependent responses found in the previous analysis.

Figure 15 presents the changes in large-scale environments over the different basins in the RegCM4 and GCM RCP8.5 simulations. The mean differences were calculated for the June–November season for the Atlantic, Western and Eastern Pacific basins, the November–March season for the Australasia domain and for the months of May, June, September–December for the North Indian Ocean. The first column shows the changes in vertical wind shear (Vs), defined as the magnitude of the vector difference of the wind at 850 and 200 hPa. Excluding the influence of other environmental factors, high values in Vs are related to reduced TC activity and intensity (Frank and Ritchie 2001; Emanuel and Nolan 2004; Camargo et al. 2007).

Focusing on the RegCM4 runs first, there are prevailing decreases in Vs over the North Indian Ocean, the Gulf of Mexico, the eastern Pacific off the Mexican coast, the Florida/Caribbean region, and the southeast Asia regions north of Australia i.e. favorable conditions for increased TC activity. Over these regions, except north of Australia, the track densities indeed increase. Conversely, Vs increases across the Australia continent, over Central America and the south Gulf of Mexico and over the western Pacific off the coast of China, which is consistent with the reduced TC activity found over these regions (Fig. 10d), with the exception of the eastern Pacific coastal areas. The projected changes in Vs, which appear to be an important factor driving the TC responses in the model, are broadly in line with those reported by Vecchi and Soden (2007) and Murakami et al. (2012a), except over the northern part of the Gulf of Mexico.

The second column shows changes in relative humidity at 700 hPa (RH700), projecting a consistent increase in mid-tropospheric RH over most regions except for the Northeastern Asia, North of Australia and central America areas. In these latter two regions, this factor appears to be dominant in inducing a decrease of TC activity (Fig. 10d), a result in line also with Vecchi and Soden (2007). Note that the changes over the Eastern Pacific are opposite to those documented by Vecchi and Soden (2007) and Murakami et al. (2012a), but they are broadly consistent with the changes in track density (Fig. 10).

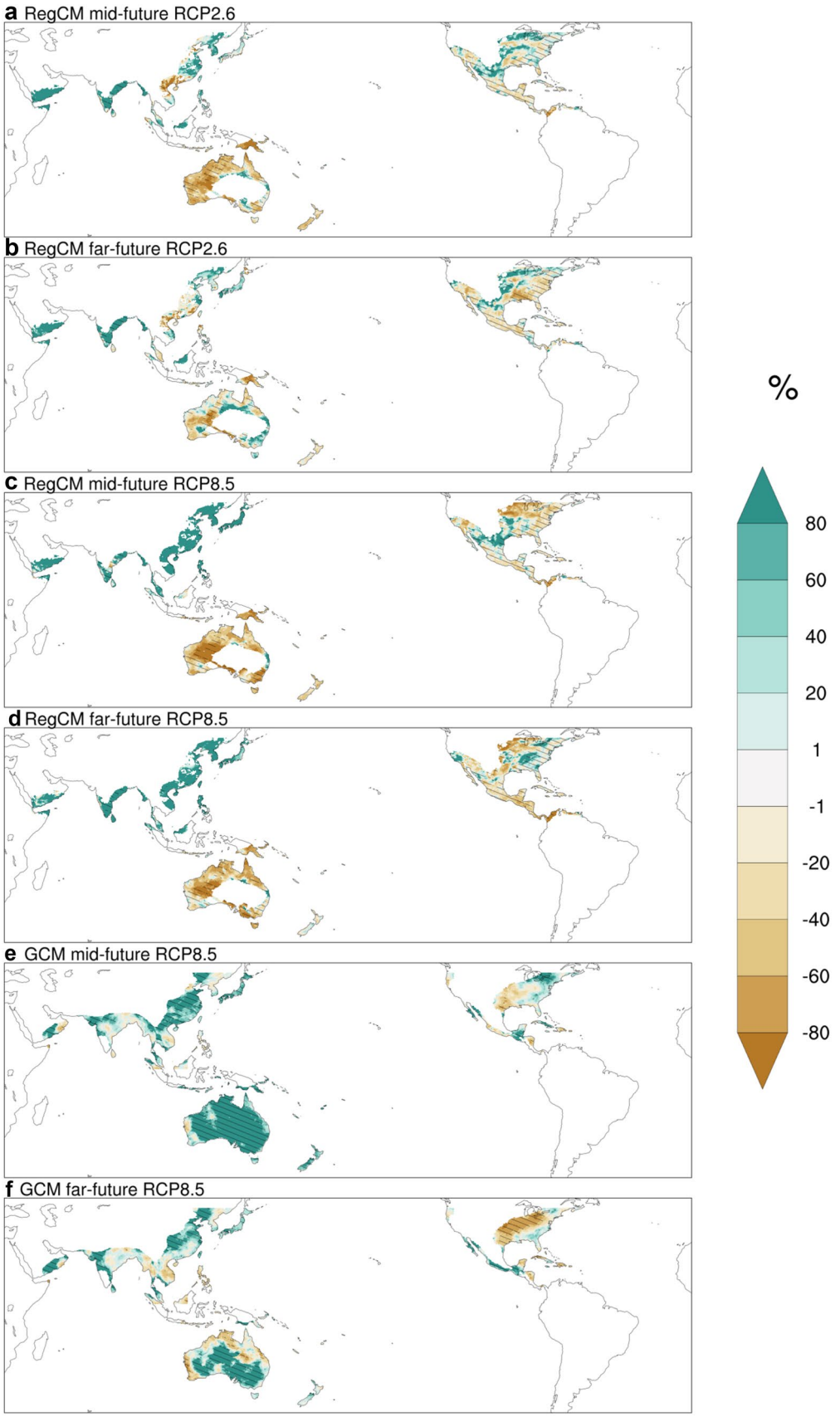

◂**Fig. 13** Changes in the total mean annual TC rainfall for the RegCM4 ensemble mean under the RCP2.6 scenario for the **a** mid- and **b** far-future; under the RCP8.5 for the **c** mid- and **d** far-future and for the GCM ensemble **e** mid- and **f** far-future. The mid-future period refers to 2041–2060 and the far-future period refers to 2080–2099. The map show regions with precipitation greater than 1 mm day^{-1} and with a track density of least 5 days in the historical period. Hatched areas show where changes are significant at a 95% level of confidence, based on the Wilcoxon rank-sum test

The third column shows the Maximum Potential Intensity (MPI; Emanuel 1995), i.e. the maximum sustainable intensity of TCs based on the thermodynamics of the atmosphere and sea surface. The RegCM4 simulations exhibit MPI increases over most TC regions (North Atlantic, Eastern Pacific, North Indian and Northwest Pacific Ocean), possibly explaining the increase in the frequency of the most intense TCs (Fig. 11). However, for Australasia, the differences in MPI between the future and historical periods are not homogenous throughout the basin. These results are consistent with those obtained by Murakami et al. (2012a) and Camargo (2013) using GCMs.

The change in the Genesis Potential Index (GPI; Emanuel and Nolan 2004; Camargo 2013) for the ensemble mean is displayed in the last column. This is a metric that estimates the potential for a TC to develop, combining the values of Vs, RH700, MPI, and large-scale vorticity. Larger values of GPI are associated with enhanced TC development. Model-projected GPI increases modestly in the North Indian Ocean and Eastern Pacific but decreases in the Caribbean and Australasia, consistent with the changes in the TC density (Figs. 10c, d). However, over the central tropical Atlantic a statistically significant decrease in track density (Fig. 10d) is noted with negligible or increasing GPI (Fig. 15). Additionally, over the tropical Northwestern Pacific a strong increase in GPI occurs in the mid-future time period, but with slightly decreasing track density in the same region (Fig. 10c). In these regions it appears that large-scale forcings not captured by the GPI parameter are causing changes to the track density. For instance, over the central tropical Atlantic it is possible that a weakening of the west African monsoon may decrease the frequency of easterly waves which are the focus of tropical cyclone development over the central tropical Atlantic. Overall, the changes presented here for GPI are similar to the projections of Vecchi and Soden (2007) and Murakami et al. (2012a), with the exception of those for the Eastern Pacific. However, the RegCM4 projections for TC frequency over the Eastern Pacific agree with most recent studies using high-resolution models (Knutson et al. 2015; Bhatia et al. 2018).

A Similar analysis for the ensemble of the GCMs (bottom panels Fig. 15), shows a prevailing, but not ubiquitous, consistency with the RegCM4 results. For both periods under the RCP8.5 scenario, there are increases in Vs and a reduction in the mid-troposphere RH over the North Atlantic Ocean, explaining the decrease in the TC development in the GCMs (Fig. 10f). Also, the MPI values show high values over the eastern Australian coast, consistent with the significant increase in the frequency of the most intense TCs (Fig. 11b). Finally, the inconsistencies in the changes in the TC activity between GCMs and RegCM4 found over the Bengal Bay and South China Sea can be explained by the projected changes in the RH700, for which the RegCM4 simulations produce a larger increase in the mid-troposphere, which then contributes to the simulated increase of TC activity.

The projected changes in seasonal mean SST and vertical wind shear from the five GCM analyzed are shown in Supplementary Figures S7 and S8, as they can help to explain the changes in the TC frequency. As expected, all the models show a global increase in SST in the range of 1–6 °C (Supplementary Figure S7), larger for the far future and for the RCP8.5 scenario. The largest warming is projected over the Northwest and Eastern Pacific basins, this latter showing also a significant increase in TC activity. Overall, the HadGEM2-ES produces the largest warming, particularly over the North Pacific Ocean.

Over the North Atlantic and Australasia, almost all the models, scenarios and periods exhibit an increase in vertical wind shear (Vs, Supplementary Figure S8), while a decrease in Vs is found over the North Indian Ocean. All these changes are broadly consistent with the changes in TC frequency. For the Northwest Pacific, the changes in Vs are small in the south of the basin, while in the north they are not consistent across scenarios and periods. Similar results are found in the Eastern Pacific Ocean.

6 Summary and conclusions

The characteristics of TC activity over four CORDEX domains including five TC regions are examined for present and future climate conditions using the regional climate model RegCM4 driven by three GCMs. We analyze results from a series of simulations conducted as part of the CORDEX-CORE program at a horizontal grid spacing of 25 km for a historical period (1995–2014) and two future periods (2041–2060 and 2080–2099) under the RCP2.6 and RCP8.5 scenarios. Overall, the RegCM4 captures most of the features of the observed TC climatology, albeit with some systematic biases, such as an overestimate of TC density in the Eastern Pacific Ocean and an underestimate in the North Indian Ocean. In general, the RegCM4 shows an improved simulation of several TC statistics compared to the driving GCMs in most basins,

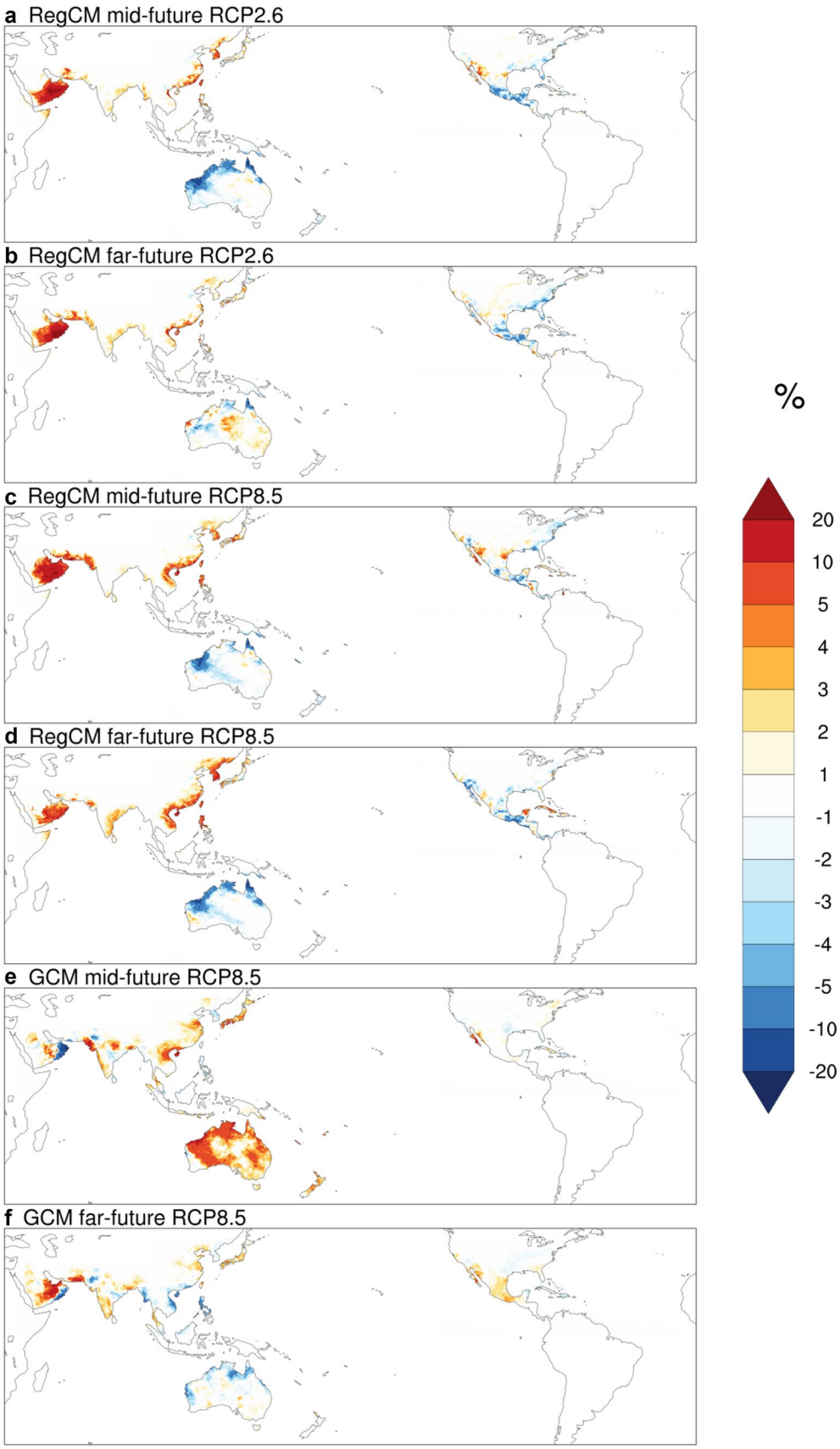

◂**Fig. 14** Changes in the contribution of TCs to extreme rainfall using the POT approach for the RegCM4 ensemble mean under the RCP2.6 scenario for the **a** mid- and **b** far-future; under the RCP8.5 for the **c** mid- and **d** far-future and for the GCM ensemble **e** mid- and **f** far-future. The mid-future period refers to 2041–2060 and the far-future period refers to 2080–2099

the main exception being the North Indian Ocean, where the GCMs produce more TCs than RegCM4 especially in the second peak season, more in line with observations.

Regarding the future scenarios, the changes in TC characteristics produced by the RegCM4 indicate prevailing increases in TC frequency between 9 and 52%, depending on the scenario and period, over the North Indian Ocean and the Eastern Pacific. This latter region also shows a longer TC season in the future (extending from April to December rather than May to November). These changes are consistent with the changes in GPI, particularly as related to an increase in mid-tropospheric relative humidity. On the other hand, the North Atlantic and Australasia basins show a decrease in TC frequency between 3 and 45%, depending on the scenario and period, mostly associated with an increase in wind shear over these basins. Over land, the changes in TC days show a prevailing increase in India and decreases in Australia, Central America and Mexico. These results are qualitatively consistent with many earlier studies based on climate projections for the late twenty-first and twenty-second Century (Emanuel et al. 2008; Lavender and Walsh 2011; Murakami et al. 2013; Diro et al. 2014; Knutson et al. 2010, 2015; Bacmeister et al. 2018), but they are opposite to those of Murakami et al. (2012b, 2014) over the northwest and northeast Pacific. The main difference between the GCMs and RegCM4 TC responses occurs over the North Indian ocean basin, where the GCMs project a decrease in TC number.

The projections show a significant increase in the frequency (> 16%) of the strongest TCs over the Eastern Pacific, the North Atlantic, Northwest Pacific and the North Indian Ocean basins where the MPI has higher values for all future scenarios. It is important to highlight that these results are robust across the simulations using different driving GCMs for RCP8.5 scenario. Over the Eastern Pacific, Australasia and North Indian Ocean, the projected changes in the duration of TCs in the RegCM4 are consistent with those documented by Webster et al. (2005) in observations and Emanuel et al. (2008), who showed a reduction in the number of long lasting TCs for future climate projections. However, the GCM and RegCM4 ensembles show different responses over Australasia, where the GCMs project a reduction in the frequency of short-duration TCs and an increase in those with a longer lifetime.

The change in total annual TC rainfall exhibits a spatial pattern similar to that of the track density, increasing significantly over the North India Ocean and decreasing in Australasia (between 3 and 10%) and southern Mexico. We also find that future TCs will have a stronger effect on the upper part of rainfall distribution over locations in the North Indian Ocean and northwestern Mexico, consistent with trends observed by Cavazos et al. (2008) and Zhang and Zhou (2019). The change in the TC rainfall rate exhibits an increase over Korea, Japan, India and the Arabian Peninsula, and a mixed signal over the eastern coast of the United States and Central America. In general, the GCM and

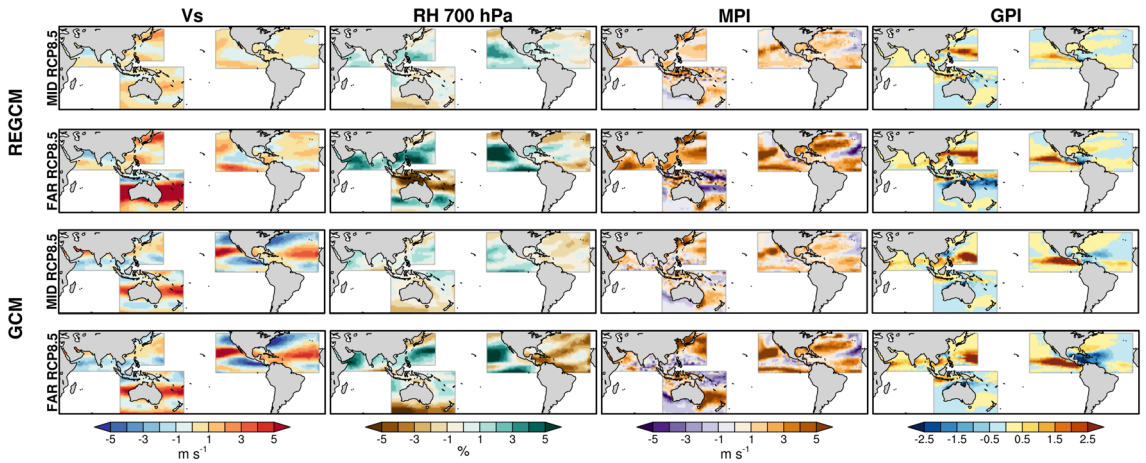

Fig. 15 Changes in large-scale environmental parameters associated with hurricane intensity and activity in terms of (left)–(right) vertical wind shear between 850 and 200 hPa (m s^{-1}), 700 hPa relative humidity (%), wind maximum potential intensity (MPI, m s^{-1}), and genesis potential index (GPI), for (top)–(bottom) the RegCM4 in the RCP8.5 for the mid- and far-future, and the GCMs in the RCP8.5 for the mid- and far-future. The mid-future period refers to 2041–2060 and the far-future period refers to 2080–2099. The mean differences were calculated for the June–November season for the Atlantic, Northwest and Eastern Pacific basins, the November–March season for the Australasia domain and for the months of May, June, September–December for the North Indian Ocean

Table 6 Tropical cyclone activity (percent change) statistics for RegCM4 ensemble (mid- or far-future vs historical period), over the regions of the Fig. 2a

Scenario	North Atlantic				Australasia				Eastern Pacific				North Indian				Northwestern Pacific			
	RCP2.6		RCP8.5		RCP2.6		RCP8.5		RCP2.6		RCP8.5		RCP2.6		RCP8.5		RCP2.6		RCP8.5	
Period	M.F.	F.F.	M.F.	F.F.	M.F.	F.F.	M.F.	F.F.	M.F.	F.F.	M.F.	F.F.	M.F.	F.F.	M.F.	F.F..	M.F.	F.F.	M.F.	F.F.
No. of TC (cat 0–5)	0	5	−3	−6	−30	−10	−38	−45	15	19	21	33	15	13	9	52	−8	−4	21	9
No. of TC (cat 3–5)	25	31	26	35	−22	1	−38	−21	22	16	31	66	22	33	0	255	−18	−65	71	40
TC rainfall (total)	17	13	−1	−6	−10	−3	−10	−10	11	8	10	−14	9	9	8	10	4	3	17	29
Contribution of TCs to extremes of precipitation	17	22	−1	−23	−27	51	−38	−42	11	32	14	−21	456	430	386	431	33	29	82	126

RegCM4 ensembles show consistent signals in mean annual TC rainfall, precipitation rate and contribution to extreme events, with the exception of Australia and Mexico, where however, the GCMs have the largest bias in mean annual TC rainfall and TC contribution to extreme precipitation during the historical period. A summary of the results for the RegCM4 simulations is found in Table 6.

Our results clearly indicate that the issue of TC responses to increased GHG forcing is a complex one, as it depends strongly on changes in the large-scale atmospheric environments forcing TC formation, and thus it is highly basin-dependent. Future work should explore more in detail the role of the vertical wind shear (Tran-Quang et al. 2020) and other environmental factors (Emanuel et al. 2004) in future changes in TC intensity. Also, while we focused on cross basin intercomparison of responses, more detailed analysis of individual basins might yield a more in depth understanding of local driving mechanisms of changes in TC activity. In addition, the limitations of using a BC approach in the calculation of the TC intensity in order to account for the lack of sufficient model resolution should be better investigated.

Some robust and statistically significant responses were found in our study, often but not always in line with previous studies, and not always consistent between the RegCM4 and driving GCMs. This implies that a robust assessment of TC changes requires analyses of large ensembles of simulations with high resolution models driven by different GCMs capable of representing the response of different TC characteristics to critical atmospheric factors. Multi-model intercomparison projects such as CORDEX, HighResMIP and CMIP6 will thus provide increasingly valuable platforms to address this critical issue for society.

Supplementary Information The online version contains supplementary material available at https://doi.org/10.1007/s00382-021-05728-6.

Acknowledgements We greatly appreciate the comments and suggestions of the editor and three anonymous reviewers, which helped improve this manuscript. The RegCM4 simulations for the ICTP institute have been completed, thanks to the support of the CINECA supercomputing center, Bologna, Italy, and ISCRA projects HP10BDU7TR and HP10BQCFJ2. The authors would like to thank Graziano Giuliani and Ivan Girotto for their constant support in the preparation of the simulations used in this paper. The authors would also like to thank the CMIP5 and Kevin Hodges, as well as the ESGF for providing access to their database, where most of the data was available. The study was also supported by the Oak Ridge Leadership Computing Facility, the National Climate-Computing Research Center at the Oak Ridge National Laboratory and the Chinese Academy of Sciences, all of whom provided access to their simulation data. The observed data were provided by NOAA (https://www.ncdc.noaa.gov/ibtracs/index.php?name=bib) and by Hylke Beck, the developer of the MSWEP data (http://www.gloh2o.org/). M. Reale has been supported in this work by OGS and CINECA under HPC-TRES award number 2015-07 and by the project FAIRSEA (Fisheries in the Adriatic Region—a Shared Ecosystem. Approach) funded by the 2014–2020 Interreg V-A Italy—Croatia CBC Programme (Standard project ID 10046951).

References

Bacmeister JT, Reed KA, Hannay C, Lawrence P, Bates S, Truesdale JE, Rosenbloom N, Levy M (2018) Projected changes in tropical cyclone activity under future warming scenarios using a high-resolution climate model. Clim Change 146:547–560. https://doi.org/10.1007/s10584-016-1750-x

Barlow M (2011) Influence of hurricane-related activity on North American extreme precipitation. Geophys Res Lett 38:L04705. https://doi.org/10.1029/2010GL046258

Beck HE, van Dijk AIJM, Levizzani V, Schellekens J, Miralles DG, Martens B, de Roo A (2017a) MSWEP: 3-hourly 0.25° global gridded precipitation (1979–2015) by merging gauge, satellite, and reanalysis data. Hydrol Earth Syst Sci 21:589–615

Beck HE et al (2017b) Global-scale evaluation of 22 precipitation datasets using gauge observations and hydrological modeling. Hydrol Earth Syst Sci 21:6201–6217

Beck HE et al (2019) Daily evaluation of 26 precipitation datasets using Stage-IV gauge-radar data for the CONUS. Hydrol Earth Syst Sc 23:207–224. https://doi.org/10.5194/hess-23-207-2019

Bengtsson L, Hodges KI, Esch M, Keenlyside N, Kornblueh L, Luo J-J, Yamagata T (2007) How may tropical cyclones change in a warmer climate? Tellus 59A:539–561

Bengtsson L, Hodges KI, Keenlyside N (2009) Will extratropical storms intensify in a warmer climate? J Clim 22(9):2276–2301. https://doi.org/10.1175/2008jcli2678.1

Bhatia K, Vecchi G, Murakami H, Underwood S, Kossin J (2018) Projected response of tropical cyclone intensity and intensification in a global climate model. J Clim 31:8281–8303. https://doi.org/10.1175/JCLI-D-17-0898.1

Bretherton CS, Park S (2009) A new moist turbulence parameterization in the community atmosphere model. J Clim 22:3422–3448

Camargo SJ (2013) Global and regional aspects of tropical cyclone activity in the CMIP5 models. J Clim 26:9880–9902. https://doi.org/10.1175/JCLI-D-12-00549.1

Camargo SJ, Wing AA (2016) Tropical cyclones in climate models. WIREs Clim Change 7:211–237. https://doi.org/10.1002/wcc373

Camargo SJ, Emanuel KA, Sobel AH (2007) Use of a genesis potential index to diagnose ENSO effects on tropical cyclone genesis. J Clim 20:4819–4834

Cavazos T, Turrent C, Lettenmaier DP (2008) Extreme precipitation trends associated with tropical cyclones in the core of the North American monsoon. Geophys Res Lett 35:L21703

Chavas DR, Emanuel KA (2010) A QuikSCAT climatology of tropical cyclone size. Geophys Res Lett 37:L18816. https://doi.org/10.1029/2010GL044558

Christensen JH, Krishna Kumar K, Aldrian E, An S-I, Cavalcanti IFA, de Castro M, Dong W, Goswami P, Hall A, Kanyanga JK, Kitoh A, Kossin J, Lau N-C, Renwick J, Stephenson DB, Xie S-P, Zhou T (2013) Climate phenomena and their relevance for future regional climate change. In: Stocker TF, Qin D, Plattner G-K, Tignor M, Allen SK, Boschung J, Nauels A, Xia Y, Bex V, Midgley PM (eds) Climate change 2013: the physical science basis. Contribution of Working Group I to the fifth assessment report of the intergovernmental panel on climate change. Cambridge University Press, p 1535

Czajkowski J, Villarini G, Michel-Kerjan E, Smith JA (2013) Determining tropical cyclone inland flooding loss on a large scale through a new flood peak ratio-based methodology. Environ Res Lett 8:044056. https://doi.org/10.1088/1748-9326/8/4/044056

Diro GT, Giorgi F, Fuentes-Franco R, Walsh KJE, Guliani G, Coppola E (2014) Tropical cyclones in a regional climate change projection with RegCM4 over the CORDEX Central America domain. Clim Change 125:79–94. https://doi.org/10.1007/s10584-014-1155-7

Dominguez C, Magaña V (2018) The role of tropical cyclones in precipitation over the tropical and subtropical North America. Front Earth Sci 6:19. https://doi.org/10.3389/feart.2018.00019

Dunne JP et al (2012) GFDL's ESM2 global coupled climate-carbon earth system models. Part I: physical formulation and baseline simulation characteristics. J Clim 25:6646–6665

Elguindi N, Giorgi F, Turuncoglu UU (2014) Assessment of CMIP5 global model simulations over the sub-set of CORDEX domains used in the Phase I CREMA Experiment. Clim Change. https://doi.org/10.1007/S10584-013-0935-9

Emanuel K (1991) A scheme for representing cumulus convection in large scale models. J Atmos Sci 48:2313–2335

Emanuel KA (1995) Sensitivity of tropical cyclones to surface exchange coefficients and a revised steady-state model incorporating eye dynamics. J Atmos Sci 52:3969–3976

Emanuel KA, Nolan D (2004) Tropical cyclone activity and the global climate system. Preprints, 26th Conf. on hurricanes and tropical meteorology, Miami, FL, Amer Meteor Soc 10(A.2). Available online at https://ams.confex.com/ams/26HURR/techprogram/paper_75463.htm

Emanuel KA, DesAutels C, Holloway C, Korty R (2004) Environmental control of tropical cyclone intensity. J Atmos Sci 61:843–858

Emanuel KA, Sundararajan R, Williams J (2008) Hurricanes and global warming: results from downscaling IPCC AR4 simulations. Bull Am Meteor Soc 89:347–367

Frank WM, Ritchie EA (2001) Effects of vertical wind shear on the intensity and structure of numerically simulated hurricanes. Mon Weather Rev 129:2249–2269

Franklin JL, Black ML, Valde K (2003) GPS dropwindsonde wind profiles in hurricanes and their operational implications. Weather Forecast 18:32–44

Fuentes-Franco R, Giorgi F, Coppola E, Zimmermann K (2017) Sensitivity of tropical cyclones to resolution, convection scheme and ocean flux parameterization over Eastern Tropical Pacific and Tropical North Atlantic Oceans in the RegCM4 model. Clim Dyn 49(1–2):547–561

Gentry MS, Lackmann GM (2010) Sensitivity of simulated tropical cyclone structure and intensity to horizontal resolution. Mon Weather Res 138:688–704

Giorgi F (2019) Thirty years of regional climate modeling: where are we and where are we going next? J Geophys Res Atmos 124:5696–5723

Giorgi F, Gutowski WJ (2015) Regional dynamical downscaling and the CORDEX initiative. Annu Rev Environ Resour 40:467–490

Giorgi F, Jones C, Asrar GR (2009) Addressing climate information needs at the regional level: the CORDEX framework. WMO Bull 58(3):175–183

Giorgi F, Coppola E, Solmon F, Mariotti L et al (2012) RegCM4: model description and preliminary tests over multiple CORDEX domains. Clim Res 52:7–29

Gleixner S, Keenlyside N, Hodges KI et al (2014) An inter-hemispheric comparison of the tropical storm response to global warming. Clim Dyn 42:2147–2157. https://doi.org/10.1007/s00382-013-1914-6

Grell GA, Dudhia J, Stauffer D (1994) A description of the fifth-generation Penn State/NCAR mesoscale model (MM5). Technical report NCAR/TN-398 + STR, National Center for Atmospheric Research

Grenier H, Bretherton CS (2001) A moist PBL parameterization for large-scale models and its application to subtropical cloud-topped marine boundary layers. Mon Weather Rev 129:357–377

Gupta S (2010) Synthesis report on ten ASEAN countries disaster risks assessment: ASEAN Disaster Risk Management Initiative. https://doi.org/10.13140/RG.2.2.32014.36160

Gutowski WJ Jr, Giorgi F, Timbal B, Frigon A, Jacob D, Kang HS, Raghavan K, Lee B, Lennard C, Nikulin G, O'Rourke E, Rixen M, Solman S, Stephenson T, Tangang F (2016) WCRP coordinated regional downscaling experiment (CORDEX): a diagnostic MIP for CMIP6. Geosci Model Dev 9:4087–4095. https://doi.org/10.5194/gmd-9-4087-2016

Hodges KI (1994) A general method for tracking analysis and its application to meteorological data. Mon Weather Rev 122:2573–2586

Hodges KI (1995) Feature tracking on the unit sphere. Mon Weather Rev 123:3458–3465

Hodges KI (1999) Adaptive constraints for feature tracking. Mon Weather Rev 127:1362–1373

Holtslag A, de Bruijn E, Pan H-L (1990) A high resolution air mass transformation model for short range weather forecasting. Mon Weather Rev 118:1561–1575

Hsu WC, Patricola CM, Chang P (2019) The impact of climate model sea surface temperature biases on tropical cyclone simulations. Clim Dyn 53:173. https://doi.org/10.1007/s00382-018-4577-5

Jin C-S, Cha D-H, Lee D-K, Suh M-S, Hong S-Y, Kang H-S, Ho C-H (2016) Evaluation of climatological tropical cyclone activity over the western North Pacific in the CORDEX-East Asia multi-RCM simulations. Clim Dyn 47:765–778. https://doi.org/10.1007/s00382-015-2869-6

Jones CD, Hughes JK, Bellouin N, Hardiman SC, Jones GS, Knight J, Liddicoat S, O'Connor FM, Andres RJ, Bell C, Boo KO, Bozzo A, Butchart N, Cadule P, Corbin KD, Doutriaux-Boucher M, Friedlingstein P, Gornall J, Gray L, Halloran PR, Hurtt G, Ingram WJ, Lamarque JF, Law RM, Meinshausen M, Osprey S, Palin EJ, Parsons Chini L, Raddatz T, Sanderson MG, Sellar AA, Schurer A, Valdes P, Wood N, Woodward S, Yoshioka M, Zerroukat M (2011) The HadGEM2-ES implementation of CMIP5 centennial simulations. Geosci Model Dev 4(3):543–570. https://doi.org/10.5194/gmd-4-543-2011

Kain J-S (2004) The Kain–Fritsch convective parameterization: an update. J Appl Meteorol 43(1):170–181

Kain J-S, Fritsch J-M (1990) A one-dimensional entraining/detraining plume model and its application in convective parameterization. J Atmos Sci 47(23):2784–2802

Khouakhi A, Villarini G, Vecchi GA (2017) Contribution of tropical cyclones to rainfall at the global scale. J Clim 30:359–372. https://doi.org/10.1175/JCLI-D-16-0298.1

Knapp KR, Kruk MC, Levinson DH, Diamond HJ, Neumann CJ (2010) The International Best Track Archive for Climate Stewardship (IBTrACS): unifying tropical cyclone best track data. Bull Am Meteor Soc 91:363–376. https://doi.org/10.1175/2009BAMS2755.1

Knapp KR, Diamond HJ, Kossin JP, Kruk MC, Schreck CJ (2018) International Best Track Archive for Climate Stewardship (IBTrACS) Project, Version 4. NOAA National Centers for Environmental Information. https://doi.org/10.25921/82ty-9e16. Accessed 10/09/2019

Knutson TR, McBride JL, Chan JCL, Emanuel KA, Holland GJ, Landsea C, Held IM, Kossin JP, Srivastava AK, Sugi M (2010) Tropical cyclones and climate change. Nat Geosci 3(3):157–163. https://doi.org/10.1038/ngeo779

Knutson TR, Sirutis JJ, Vecchi GA, Garner S, Zhao M, Kim H-S, Bender M, Tuleya RE, Held IM, Villarini G (2013) Dynamical downscaling projections of late 21st century Atlantic hurricane activity: CMIP3 and CMIP5 model-based scenarios. J Clim 26:6591–6617. https://doi.org/10.1175/JCLI-D-12-00539.1

Knutson TR et al (2015) Global projections of intense tropical cyclone activity for the late twenty-first century from dynamical downscaling of CMIP5/RCP4.5 scenarios. J Clim 28(18):7203–7224. https://doi.org/10.1175/JCLI-D-15-0129.1

Knutson T, Camargo SJ, Chan JC, Emanuel K, Ho C, Kossin J, Mohapatra M, Satoh M, Sugi M, Walsh K, Wu L (2019) Tropical cyclones and climate change assessment: Part I: detection and attribution. Bull Am Meteor Soc 100:1987–2007. https://doi.org/10.1175/BAMS-D-18-0189.1

Knutson T, Camargo SJ, Chan JC, Emanuel K, Ho C, Kossin J, Mohapatra M, Satoh M, Sugi M, Walsh K, Wu L (2020) Tropical cyclones and climate change assessment: Part II. Projected response to anthropogenic warming. Bull Am Meteor Soc. https://doi.org/10.1175/BAMS-D-18-0194.1

Kruk MC, Knapp KR, Levinson DH (2010) A technique for combining global tropical cyclone best track data. J Atmos Oceanic Technol 27:680–692. https://doi.org/10.1175/2009JTECHA1267.1

Lavender SL, Walsh KJE (2011) Dynamically downscaled simulations of Australian region tropical cyclones in current and future climates. Geophys Res Lett. https://doi.org/10.1029/2011GL047499

Li T, Kwon M, Zhao M, Kug J-S, Luo J-J, Yu W (2010) Global warming shifts Pacific tropical cyclone location. Geophys Res Lett 37:L21804

Liu M, Vecchi GA, Smith JA, Murakami H (2018) Projection of landfalling-tropical cyclone rainfall in the Eastern United States under anthropogenic warming. J Clim 31:7269–7286. https://doi.org/10.1175/JCLI-D-17-0747.1

Liu J, Shangguan D, Liu S, Ding Y, Wang S, Wang X (2019) Evaluation and comparison of CHIRPS and MSWEP daily-precipitation products in the Qinghai-Tibet Plateau during the period of 1981–2015. Atmos Res 230:104634

Manganello JV, Hodges KI, Kinter JL, Cash BA, Marx L, Jung T, Achuthavarier D, Adams JM, Altshuler EL, Huang B, Jin EK, Stan C, Towers P, Wedi N (2012) Tropical cyclone climatology in a 10 km global atmospheric GCM: toward weather-resolving climate modeling. J Clim 25:3867–3893

Manganello JV, Hodges KI, Dirmeyer B, Kinter JL, Cash BA, Marx L, Jung T, Achuthavarier D, Adams JM, Altshuler EL, Huang B, Jin EK, Towers P, Wedi N (2014) Future changes in the western North Pacific tropical cyclone activity projected by a multidecadal simulation with a 16-km global atmospheric GCM. J Clim 27:7622–7646. https://doi.org/10.1175/JCLI-D-13-00678.1

Martínez-Sanchez JN, Cavazos T (2014) Eastern Tropical Pacific hurricane variability and landfalls on Mexican coasts. Clim Res 58:221–234

Moss R et al (2008) Towards new scenarios for analysis of emissions, climate change, impacts, and response strategies. Intergovernmental Panel on Climate Change, Geneva, p 132

Murakami H, Wang Y, Yoshimura H, Mizuta R, Sugi M, Shindo E, Adachi Y, Yukimoto S, Hosaka M, Kusunoki S, Ose T, Kitoh A (2012a) Future changes in tropical cyclone activity projected by the new high-resolution MRI-AGCM. J Clim 25:3237–3260

Murakami H, Mizuta R, Shindo E (2012b) Future changes in tropical cyclone activity projected by multi-physics and multi-SST ensemble experiments using the 60-km-mesh MRI AGCM. Clim Dyn 39(9–10):2569–2584

Murakami H, Sugi M, Kitoh A (2013) Future changes in tropical cyclone activity in the North Indian Ocean projected by high-resolution MRI-AGCMs. Clim Dyn 40:1949–1968. https://doi.org/10.1007/s00382-012-1407-z

Murakami H, Hsu P-C, Arakawa O, Li T (2014) Influence of model biases on projected future changes in tropical cyclone frequency of occurrence. J Clim 27:2159–2181

Murakami HG, Vecchi A, Underwood S (2017) Increasing frequency of extremely severe cyclonic storms over the Arabian Sea. Nat Clim Change 7:885–889

Pal J-S, Small E-E, Eltahir E-A-B (2000) Simulation of regional scale water and energy budgets: representation of subgrid cloud and precipitation processes within RegCM. J Geophys Res 105(D24):29579–29594

Pfahl S, Wernli H (2012) Quantifying the relevance of cyclones for precipitation extremes. J Clim 25:6770–6780

Prat OP, Nelson BR (2013) Mapping the world's tropical cyclone rainfall contribution over land using the TRMM Multi-satellite precipitation analysis. Water Resour Res 49:7236–7254. https://doi.org/10.1002/wrcr.20527

Rappaport EN (2000) Loss of life in the United States associated with recent Atlantic tropical cyclones. Bull Am Meteor Soc 81:2065–2073. https://doi.org/10.1175/1520-0477(2000)0812.3.CO;2

Rastogi D, Ashfaq M, Leung R, Ghosh S, Saha A, Hodges K, Evans K (2018) Characteristics of Bay of Bengal, monsoon depressions in the 21st century. Geophys Res Lett. https://doi.org/10.1029/2018GL078756

Reed KA, Bacmeister JT, Rosenbloom NA et al (2015) Impact of the dynamical core on the direct simulation of tropical cyclones in a high-resolution global model. Geophys Res Lett 42:3603–3608. https://doi.org/10.1002/2015GL063974

Satgé F, Defrance D, Sultan B, Bonnet MP, Seyler F, Rouché N, Pierron F, Paturel JE (2020) Evaluation of 23 gridded precipitation datasets across West Africa. J Hydrol 581:124412

Seiler C, Zwiers F, Hodges KI, Scinocca J (2018) How does dynamical downscaling affect model biases and future projections of explosive extratropical cyclones along North America's Atlantic coast? Clim Dyn 50:677–692. https://doi.org/10.1007/s00382-017-3634-9

Stevens B, Giorgetta M, Esch M et al (2013) Atmospheric component of the MPI-M earth system model: ECHAM6. J Adv Model Earth Syst 5:146–172. https://doi.org/10.1002/jame.20015

Sugi M, Murakami H, Yoshida K (2017) Projection of future changes in the frequency of intense cyclones. Clim Dyn 49:619–632. https://doi.org/10.1007/s00382-016-3361-7

Taylor KE, Stouffer RJ, Meehl GA (2012) An overview of CMIP5 and the experiment design. Bull Am Meteorol Soc 78:485–498

Tiedtke M (1996) An extension of cloud-radiation parameterization in the ECMWF model: the representation of subgrid-scale variations of optical depth. Mon Weather Rev 124:745–750. https://doi.org/10.1175/1520-0493(1996)124%3C0745:AEOCRP%3E2.0.CO;2

Tran-Quang D, Pham-Thanh H, Vu T, Kieu C, Phan-Van T (2020) Climatic shift of the tropical cyclone activity affecting Vietnam's coastal region. J Appl Meteor Climatol 59:1755–1768. https://doi.org/10.1175/JAMC-D-20-0021.1

Vecchi GA, Soden BJ (2007) Increased tropical Atlantic wind shear in model projections of global warming. Geophys Res Lett 34:L08702

Vecchi GA, Delworth T, Gudgel R, Kapnick S, Rosati A, Wittenberg AT, Zeng F, Anderson W, Balaji V, Dixon K, Jia L, Kim H, Krishnamurthy L, Msadek R, Stern WF, Underwood SD, Villarini G, Yang X, Zhang S (2014) On the seasonal forecasting of regional tropical cyclone activity. J Clim 27:7994–8016. https://doi.org/10.1175/JCLI-D-14-00158.1

Vishnu S, Sanjay J, Krishnan R (2019) Assessment of climatological tropical cyclone activity over the north Indian Ocean in the CORDEX-South Asia regional climate models. Clim Dyn 53:5101. https://doi.org/10.1007/s00382-019-04852-8

Walsh KJE, Fiorino M, Landsea CW, McInnes KL (2007) Objectively determined resolution-dependent threshold criteria for the detection of tropical cyclones in climate model and reanalyses. J Clim 20:2307–2314

Walsh K, Lavender S, Murakami H, Scoccimarro E, Caron L-P, Ghantous M (2010) The tropical intercomparison project. In: Elsner JB, Hodges RE, Malmstadt JC, Scheitlin KN (eds) Hurricanes and climate change. Springer, Berlin, pp 1–24

Walsh KJE, McBride JL, Klotzbach PJ, Balachandran S, Camargo SJ, Holland G, Knutson TR, Kossin JP, Lee T-C, Sobel A, Sugi M (2016) Tropical cyclones and climate change. Wiley Interdiscip Rev Clim Change 7(1):65–89. https://doi.org/10.1002/wcc.371

Wang C, Liang J, Hodges KI (2017) Projections of tropical cyclones affecting Vietnam under climate change: downscaled HadGEM2-ES using PRECIS 2.1. Q J R Meteorol Soc. https://doi.org/10.1002/qj.3046

Watanabe M et al (2010) Improved climate simulation by MIROC5: mean states, variability, and climate sensitivity. J Clim 23:6312–6335

Webster PJ, Holland GJ, Curry JA, Chang HR (2005) Changes in tropical cyclone number, duration, and intensity in a warming environment. Science 309(5742):1844–1846. https://doi.org/10.1126/science.1116448

Wehner MF, Reed KA, Loring B, Stone D, Krishnan H (2018) Changes in tropical cyclones under stabilized 1.5 °C and 2.0 °C global warming scenarios as simulated by the Community Atmospheric Model under the HAPPI protocols. Earth Syst Dyn 9:187–195

Zappa G, Hawcroft MK, Shaffrey L, Black E, Brayshaw DJ (2015) Extratropical cyclones and the projected decline of winter Mediterranean precipitation in the CMIP5 models. Clim Dyn 45:1727–1738

Zeng X, Zhao M, Dickinson R-E (1998) Intercomparison of bulk aerodynamic algorithms for the computation of sea surface fluxes using TOGA COARE and TAO data. J Clim 11(10):2628–2644

Zhang W, Zhou T (2019) Significant increases in extreme precipitation and the associations with global warming over the global land monsoon regions. J Clim 32:8465–8488. https://doi.org/10.1175/JCLI-D-18-0662.1

Zhang ZS et al (2012) Pre-industrial and mid-Pliocene simulations with NorESM-L. Geosci Model Dev 5:523–533. https://doi.org/10.5194/gmd-5-523-2012

Zhang W, Villarini G, Vecchi GA, Murakami H (2019) Rainfall from tropical cyclones: high-resolution simulations and seasonal forecasts. Clim Dyn. https://doi.org/10.1007/s00382-018-4446-2

Zhao M, Held IM (2010) An analysis of the effect of global warming on the intensity of Atlantic hurricanes using a GCM with statistical refinement. J Clim 23:6382–6393

Terms and Conditions

Springer Nature journal content, brought to you courtesy of Springer Nature Customer Service Center GmbH (“Springer Nature”).
Springer Nature supports a reasonable amount of sharing of research papers by authors, subscribers and authorised users (“Users”), for small-scale personal, non-commercial use provided that all copyright, trade and service marks and other proprietary notices are maintained. By accessing, sharing, receiving or otherwise using the Springer Nature journal content you agree to these terms of use (“Terms”). For these purposes, Springer Nature considers academic use (by researchers and students) to be non-commercial.
These Terms are supplementary and will apply in addition to any applicable website terms and conditions, a relevant site licence or a personal subscription. These Terms will prevail over any conflict or ambiguity with regards to the relevant terms, a site licence or a personal subscription (to the extent of the conflict or ambiguity only). For Creative Commons-licensed articles, the terms of the Creative Commons license used will apply.
We collect and use personal data to provide access to the Springer Nature journal content. We may also use these personal data internally within ResearchGate and Springer Nature and as agreed share it, in an anonymised way, for purposes of tracking, analysis and reporting. We will not otherwise disclose your personal data outside the ResearchGate or the Springer Nature group of companies unless we have your permission as detailed in the Privacy Policy.
While Users may use the Springer Nature journal content for small scale, personal non-commercial use, it is important to note that Users may not:

1. use such content for the purpose of providing other users with access on a regular or large scale basis or as a means to circumvent access control;
2. use such content where to do so would be considered a criminal or statutory offence in any jurisdiction, or gives rise to civil liability, or is otherwise unlawful;
3. falsely or misleadingly imply or suggest endorsement, approval , sponsorship, or association unless explicitly agreed to by Springer Nature in writing;
4. use bots or other automated methods to access the content or redirect messages
5. override any security feature or exclusionary protocol; or
6. share the content in order to create substitute for Springer Nature products or services or a systematic database of Springer Nature journal content.

In line with the restriction against commercial use, Springer Nature does not permit the creation of a product or service that creates revenue, royalties, rent or income from our content or its inclusion as part of a paid for service or for other commercial gain. Springer Nature journal content cannot be used for inter-library loans and librarians may not upload Springer Nature journal content on a large scale into their, or any other, institutional repository.
These terms of use are reviewed regularly and may be amended at any time. Springer Nature is not obligated to publish any information or content on this website and may remove it or features or functionality at our sole discretion, at any time with or without notice. Springer Nature may revoke this licence to you at any time and remove access to any copies of the Springer Nature journal content which have been saved.
To the fullest extent permitted by law, Springer Nature makes no warranties, representations or guarantees to Users, either express or implied with respect to the Springer nature journal content and all parties disclaim and waive any implied warranties or warranties imposed by law, including merchantability or fitness for any particular purpose.
Please note that these rights do not automatically extend to content, data or other material published by Springer Nature that may be licensed from third parties.
If you would like to use or distribute our Springer Nature journal content to a wider audience or on a regular basis or in any other manner not expressly permitted by these Terms, please contact Springer Nature at

onlineservice@springernature.com